



PERGAMON

International Journal of Multiphase Flow 25 (1999) 1263–1303

International Journal of
**Multiphase
Flow**

www.elsevier.com/locate/ijmulflow

Breakup of a liquid drop suddenly exposed to a high-speed airstream

D.D. Joseph*, J. Belanger, G.S. Beavers

Department of Aerospace Engineering and Mechanics, University of Minnesota, Minneapolis, MN 55455, USA

Received 9 November 1998; received in revised form 10 April 1999

This paper is dedicated to Gad Hetsroni, on the occasion of his 65th birthday, to honor his many contributions to the understanding of multiphase flows.

Abstract

The breakup of viscous and viscoelastic drops in the high speed airstream behind a shock wave in a shock tube was photographed with a rotating drum camera giving one photograph every 5 μs . From these photographs we created movies of the fragmentation history of viscous drops of widely varying viscosity, and viscoelastic drops, at very high Weber and Reynolds numbers. Drops of the order of one millimeter are reduced to droplet clouds and possibly to vapor in times less than 500 μs . The movies may be viewed at http://www.aem.umn.edu/research/Aerodynamic_Breakup. They reveal sequences of breakup events which were previously unavailable for study. Bag and bag-and-stamen breakup can be seen at very high Weber numbers, in the regime of breakup previously called ‘catastrophic’. The movies allow us to generate precise displacement–time graphs from which accurate values of acceleration (of orders 10^4 to 10^5 times the acceleration of gravity) are computed. These large accelerations from gas to liquid put the flattened drops at high risk to Rayleigh–Taylor instabilities. The most unstable Rayleigh–Taylor wave fits nearly perfectly with waves measured on enhanced images of drops from the movies, but the effects of viscosity cannot be neglected. Other features of drop breakup under extreme conditions, not treated here, are available on our Web site. © 1999 Elsevier Science Ltd. All rights reserved.

Keywords: Drop breakup; High-speed airstream; Viscous drops; Viscoelastic drops

* Corresponding author. Tel.: +1-612-625-0309; fax: +1-612-626-1558.

1. Fragmentation of Newtonian and viscoelastic drops

The problem of aerodynamic breakup of liquid drops has given rise to a large literature. Most of the early literature focuses on drops of Newtonian liquids in subsonic airstreams, and is excellently reviewed by Pilch and Erdman (1987), and Hsiang and Faeth (1992). Shock tube studies of the breakup of Newtonian drops, usually water, under high subsonic and supersonic conditions were carried out by Hanson and Domich (1956), Engel (1958), Hanson et al. (1963), Ranger and Nicholls (1969), Reinecke and McKay (1969), Reinecke and Waldman (1970), Reinecke and Waldman (1975), Waldman et al. (1972), Simpkins and Bales (1972), Wierzba and Takayama (1988), Yoshida and Takayama (1990), Hirahara and Kawahashi (1992), and others. The excellent study of Engel (1958) showed that water drops of millimeter diameter would be reduced to mist by the flow behind an incident shock moving at Mach numbers in the range 1.3–1.7. Many of the other aforementioned studies allude to the presence of large amounts of mist. Joseph et al. (1996) argued that mist could arise from condensed vapor under flash vaporization due to (1) low pressures at the leeside produced by rarefaction and drop acceleration, (2) high tensions produced by extensional motions in the liquid stripped from the drop, (3) the frictional heating by rapid rates of deformation, and (4) the heating of sheets and filaments torn from the drop by hot air. Though mist and vapor formation is not the focus of this study, it is relevant that the Rayleigh–Taylor instability pumps fingers of hot gas, behind the shock, into the drop increasing both the frictional heating and the area of liquid surface exposed to hot gas.

The recent and fairly extensive literature on atomization is well represented in the papers by Hsiang and Faeth (1992), Hwang et al. (1996), and Faeth (1996). These results, and earlier drop breakup studies such as Krzeczowski (1980), Wierzba (1990), Kitscha and Kocamustafaogullari (1989), and Stone (1994), are restricted to relatively low Weber and Reynolds numbers. The highest Weber and Reynolds data for drop breakup was reported by Hsiang and Faeth (1992) who worked under conditions for which the Weber numbers ranged from 0.5 to 1000 with Reynolds numbers from 300 to 1600.

High Weber number drop breakup data were obtained by Engel (1958), Ranger and Nicholls (1969), and Reinecke and Waldman (1970) for air and water only, so viscous effects could not be studied. In contrast, the data presented here cover a wide range of viscosities (from 0.001 to 35 kg/m s) and a wide range of high Weber numbers (from 11,700 to 169,000), Ohnesorge numbers (from 0.002 to 82.3) and Reynolds numbers (from 40,000 to 127,600), based on the free stream conditions. Another feature, which distinguishes our experiments from previous ones, is that we have recorded all of the data as real time movies which may be seen under ‘video animations’ at our Web address. The movies capture events which were previously unknown, such as bag breakup and bag-and-stamen breakup of high viscosity drops at very high Weber numbers, whereas short wave Rayleigh–Taylor corrugations appear on water drops under similar free stream conditions (see Fig. 19).

The thesis of this paper is that breakup at high accelerations, corresponding to high Weber numbers, is controlled at early times by Rayleigh–Taylor instabilities. We back up this claim by comparing theory with experiment. From the movies, we get accurate displacement–time graphs, one point every 5 μ s, from which the huge accelerations which drive Rayleigh–Taylor instabilities can be measured. The movie frames can be processed for images of unstable waves from which the length of the most dangerous wave can be measured and compared with theory.

Only a few studies of the breakup of viscoelastic drops have been published; Lane (1951), Wilcox et al. (1961), Matta and Tytus (1982), Matta et al. (1983). Matta and co-workers did studies at Mach numbers near one and less. They showed that threads and ligaments of liquid arise immediately after breakup, rather than the droplets which are seen in Newtonian liquids. We have verified these general observations for more and different liquids in high speed air behind shocks with Mach numbers as high as 3. These structures can be seen in the photographs in Figs. 1–13 of this paper, which show just a few frames from the respective movies on our web page. For example, compare Fig. 1, which shows the breakup of a water drop in our shock tube at a shock Mach number of 2, with Figs. 5 and 7 which show, respectively, the breakup under the same conditions of a 2% aqueous solution of polyox and a

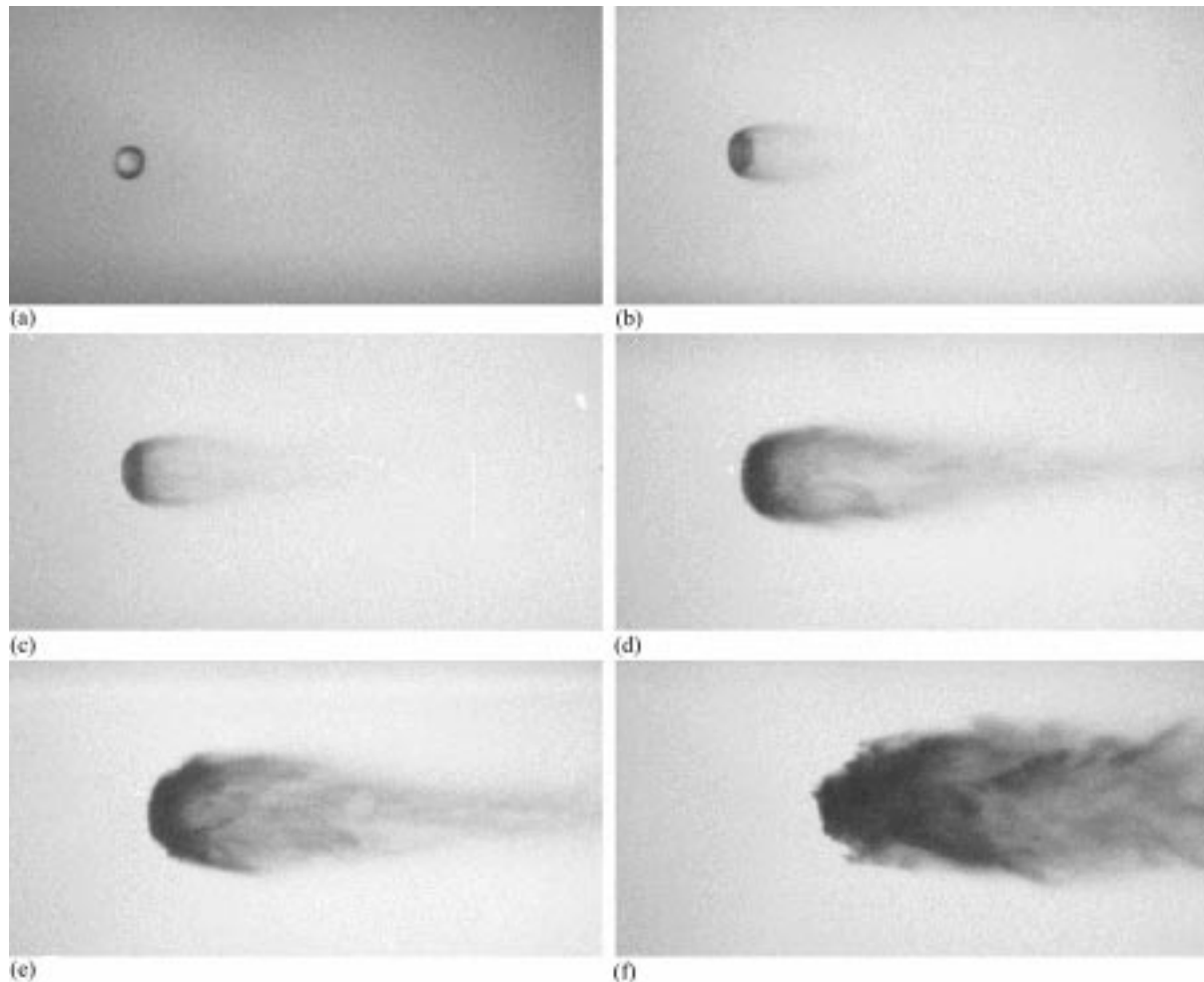


Fig. 1. Stages in the breakup of a water drop (diameter = 2.6 mm) in the flow behind a Mach 2 shock wave. Air velocity = 432 m/s; dynamic pressure = 158.0 kPa; Weber No. = 11,700. Time (μs): (a) 0, (b) 45, (c) 70, (d) 135, (e) 170, (f) 290.

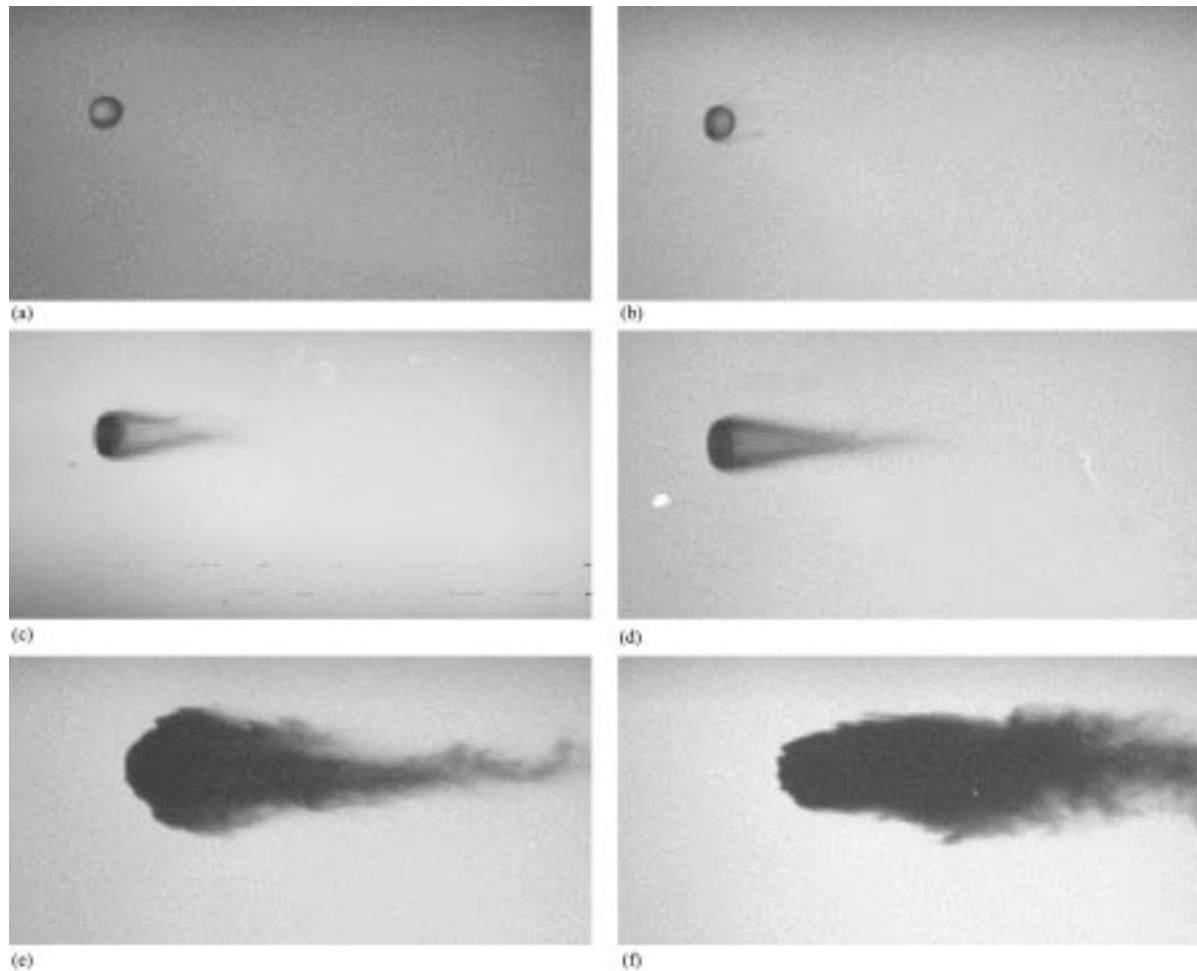


Fig. 2. Stages in the breakup of a water drop (diameter = 2.5 mm) in the flow behind a Mach 3 shock wave. Air velocity = 764 m/s; dynamic pressure = 606.4 kPa; Weber No. = 43,330. Time (μs): (a) 0, (b) 15, (c) 30, (d) 40, (e) 95, (f) 135.

2.6% solution of polystyrene butylacrylate in tributyl phosphate. Figs. 2, 6 and 8 show the breakup of the same liquids at a shock Mach number of 3.

2. Shock tube

The shock tube consists of a driver section that can be varied in length between 1.829 and 4.627 m, a double-diaphragm section, a low pressure channel with a maximum length of 10.363 m, a windowed test-section approximately 0.76 m in length, and a dump tank with a volume of approximately 1.13 m³. Both the driver section and the channel are built up from sections of extruded 6063-T6 aluminum.

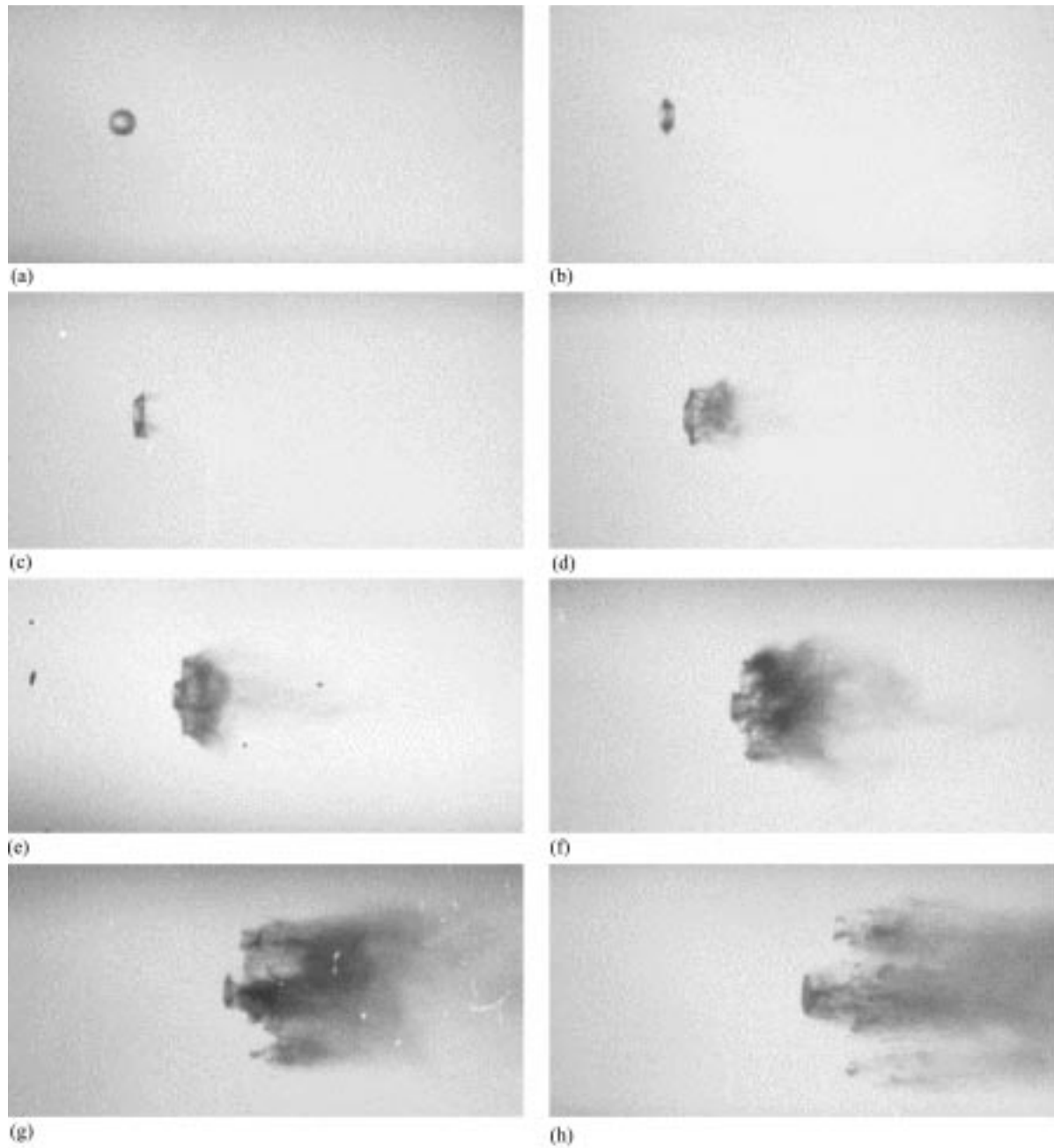


Fig. 3. Stages in the breakup of a glycerine drop (diameter = 2.3 mm) in the flow behind a Mach 2 shock wave. Air velocity = 428 m/s; dynamic pressure = 145.8 kPa; Weber No. = 10,600. Time (μs): (a) 0, (b) 70, (c) 115, (d) 165, (e) 220, (f) 250, (g) 295, (h) 345.

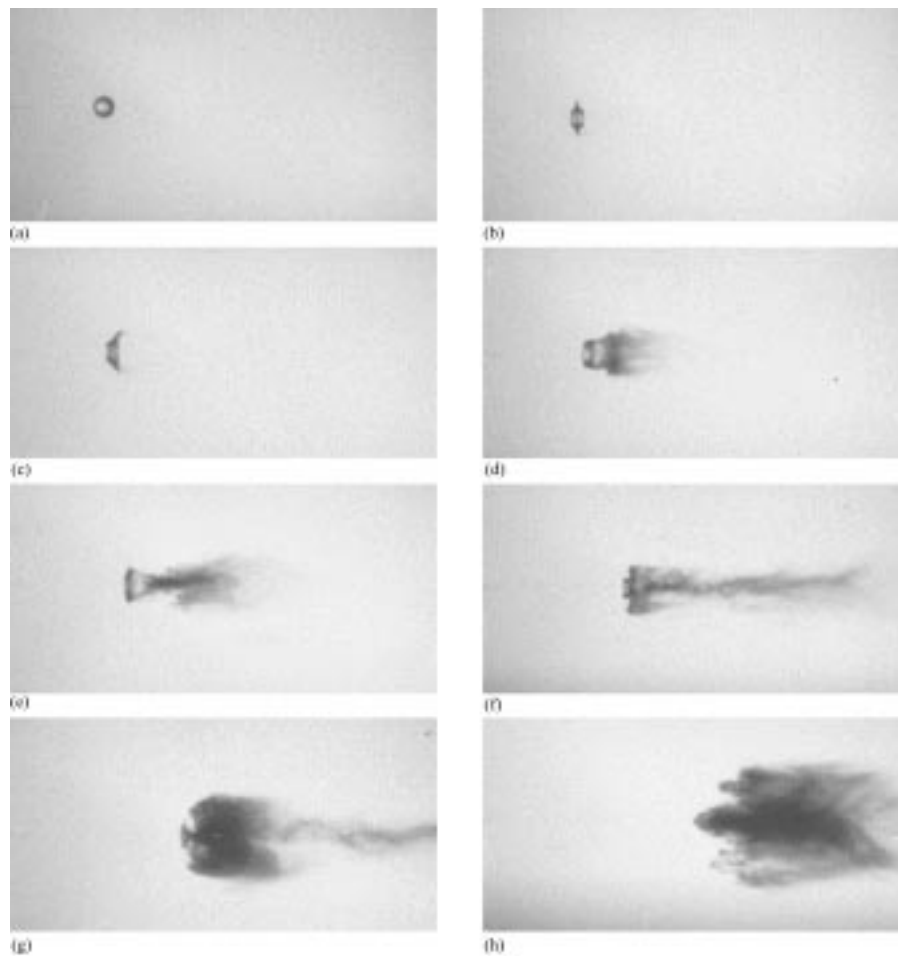


Fig. 4. Stages in the breakup of a drop of glycerine (diameter = 2.4 mm) in the flow behind a Mach 3 shock wave. Air velocity = 758 m/s; dynamic pressure = 554.0 kPa; Weber No. = 42,220. Time (μs): (a) 0, (b) 35, (c) 50, (d) 70, (e) 90, (f) 125, (g) 150, (h) 185.

The complete tube (driver, diaphragm, channel, and test section) is supported by ball-bearing carriages which ride on a precision rail. The rail in turn is mounted on a 0.152 m aluminum I-beam, which is attached through leveling screws to a set of five concrete columns. This arrangement allows for accurate leveling of the whole tube, while giving ease of movement to the complete tube system for replacement of the diaphragms and for accommodating different lengths of the system.

The tube has an internal cross-sectional shape consisting of flat side walls and semi-circular upper and lower walls, while the outside of the tube has a circular cross-section 0.127 m in diameter. This configuration was selected to keep the stresses in the walls as low as possible and to give the greatest flow area for the cross-section that could be extruded, while retaining flat side walls for continuity with the windows in the test section. The distance between the flat side walls is 0.0762 m; the upper and lower walls are semi-circular arcs with diameter 0.0955 m.

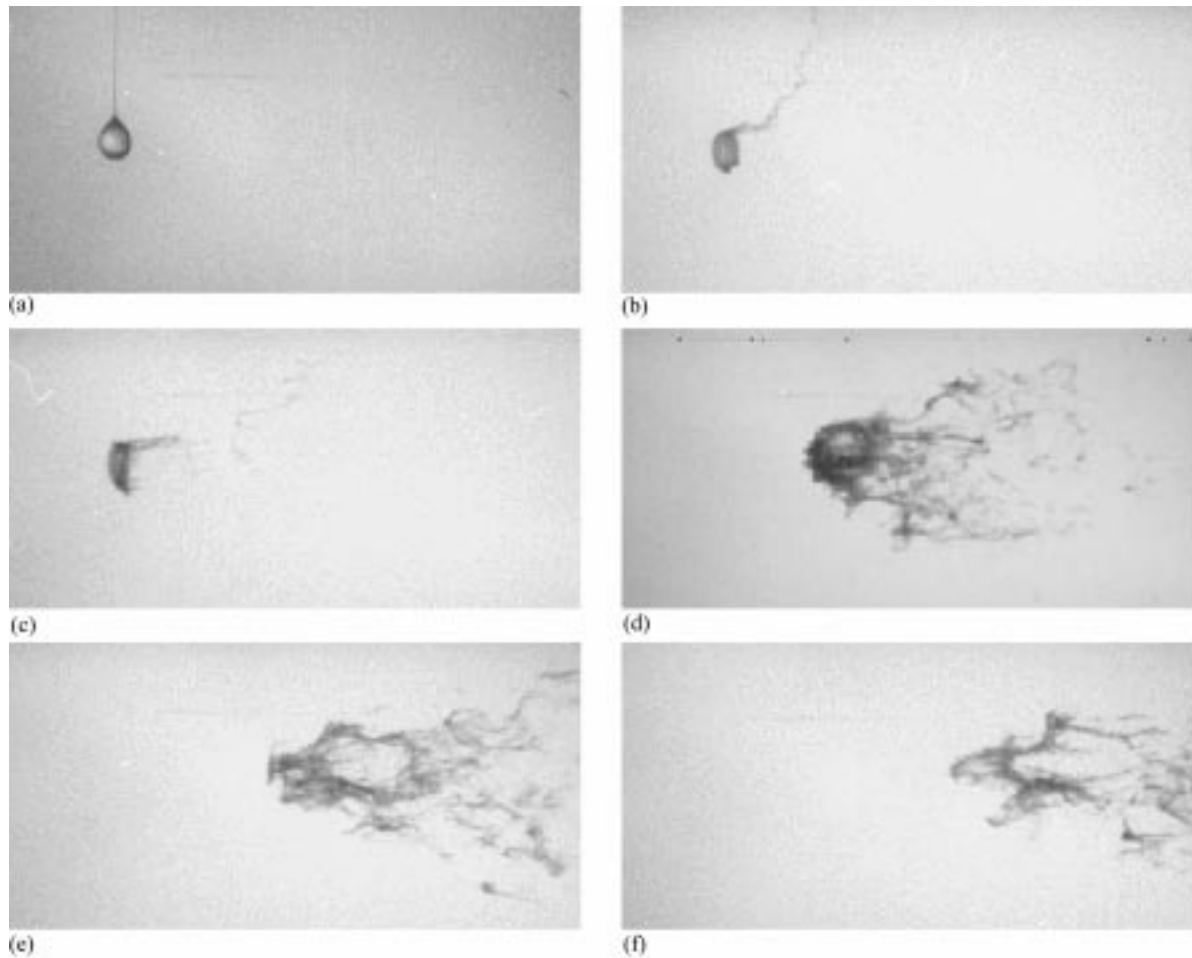


Fig. 5. Stages in the breakup of a drop of 2% aqueous solution of polyox (WSR 301; diameter = 2.9 mm) in the flow behind a Mach 2 shock wave. Air velocity = 432 m/s; dynamic pressure = 165.5 kPa; Weber No. = 15,200. Time (μ s): (a) 0, (b) 55, (c) 95, (d) 290, (e) 370, (f) 435.

The test section is built around a 0.762 m length of the extruded aluminum tube, and is designed to prevent any distortion under internal pressure, thus allowing 0.035 m long glass windows to be used. The test section incorporates flat upper and lower external surfaces, thereby facilitating the mounting of auxiliary equipment, such as the drop injection system.

The shock tube is fired by means of a double diaphragm system in which the inter-diaphragm space is filled with helium at a pressure approximately equal to the mean of the driver and channel pressures, and is evacuated through a fast-acting solenoid valve, providing a fast and repeatable firing of the shock tube.

For the experiments described in this paper, the channel pressure (air) was evacuated to 50 kPa for the Mach 3 experiments and 58 kPa for the Mach 2 experiments, and the Mach number was fixed through the driver pressure, using nitrogen for the Mach 2 tests and helium

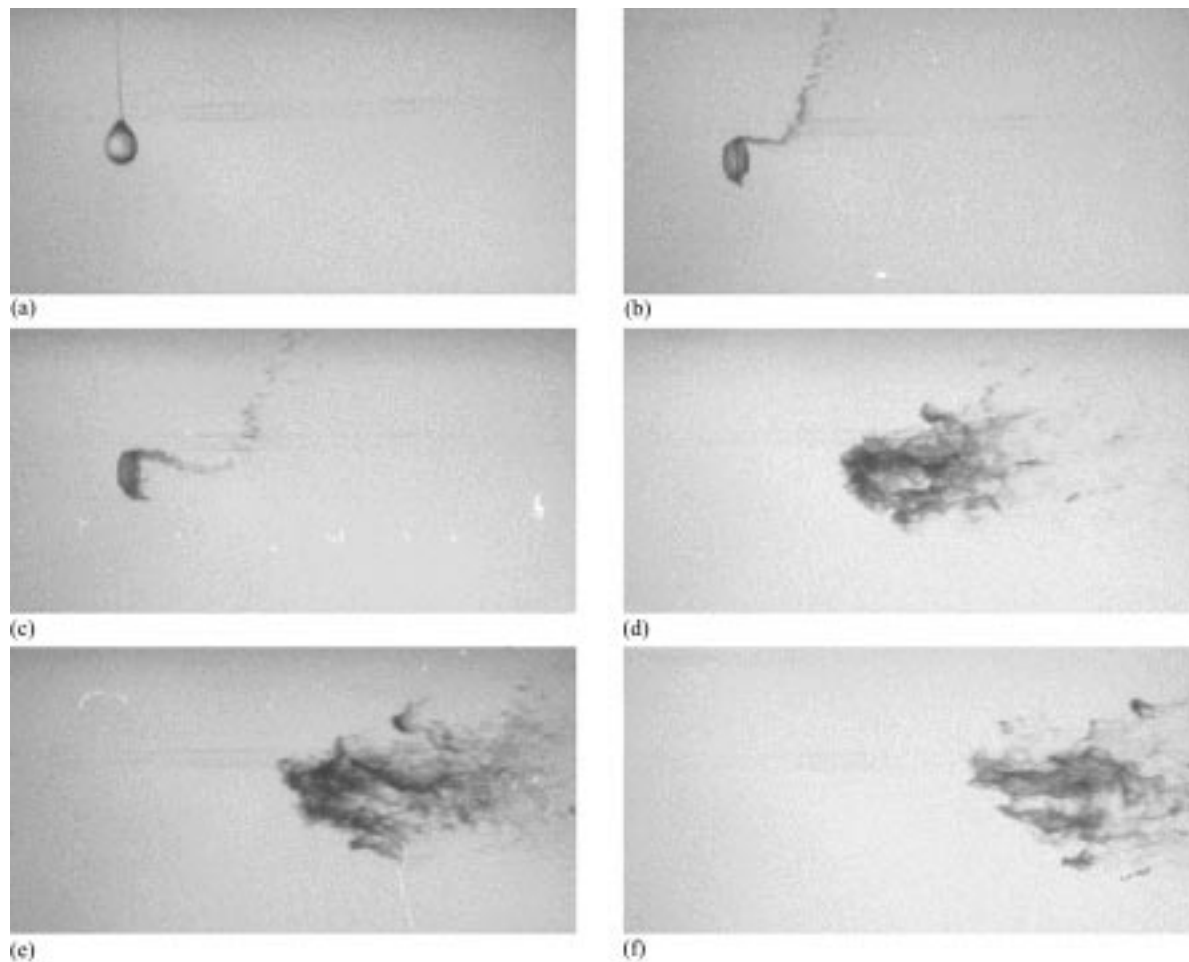


Fig. 6. Stages in the breakup of a drop of 2% aqueous solution of polyox (WSR 301; diameter = 2.9 mm) in the flow behind a Mach 3 shock wave. Air velocity = 755 m/s; dynamic pressure = 587.2 kPa; Weber No. = 54,100. Time (μ s): (a) 0, (b) 30, (c) 45, (d) 170, (e) 195, (f) 235.

for the Mach 3 tests. A drop of test liquid of known volume is injected into the test section by means of an injector device mounted on top of the test section. The injector consists of a hypodermic syringe connected by a flexible tube to a hypodermic tube which passes through a solenoid and projects into the test section from above. The syringe, flexible tube, and solenoid are enclosed within a housing, which is maintained at the channel pressure. The displacement of the syringe plunger is controlled by a micrometer which projects through the top of the injector housing. A drop of known volume is formed at the end of the injection tube. When the drop falls from the tube it is detected by a photodetector which initiates the signals, with appropriate delays, to fire the shock tube, activate the solenoid to withdraw the injector tube from the test section, and open the camera shutter. A pressure transducer near the test section is used to detect the shock wave and fire the flash lamp to take the pictures.

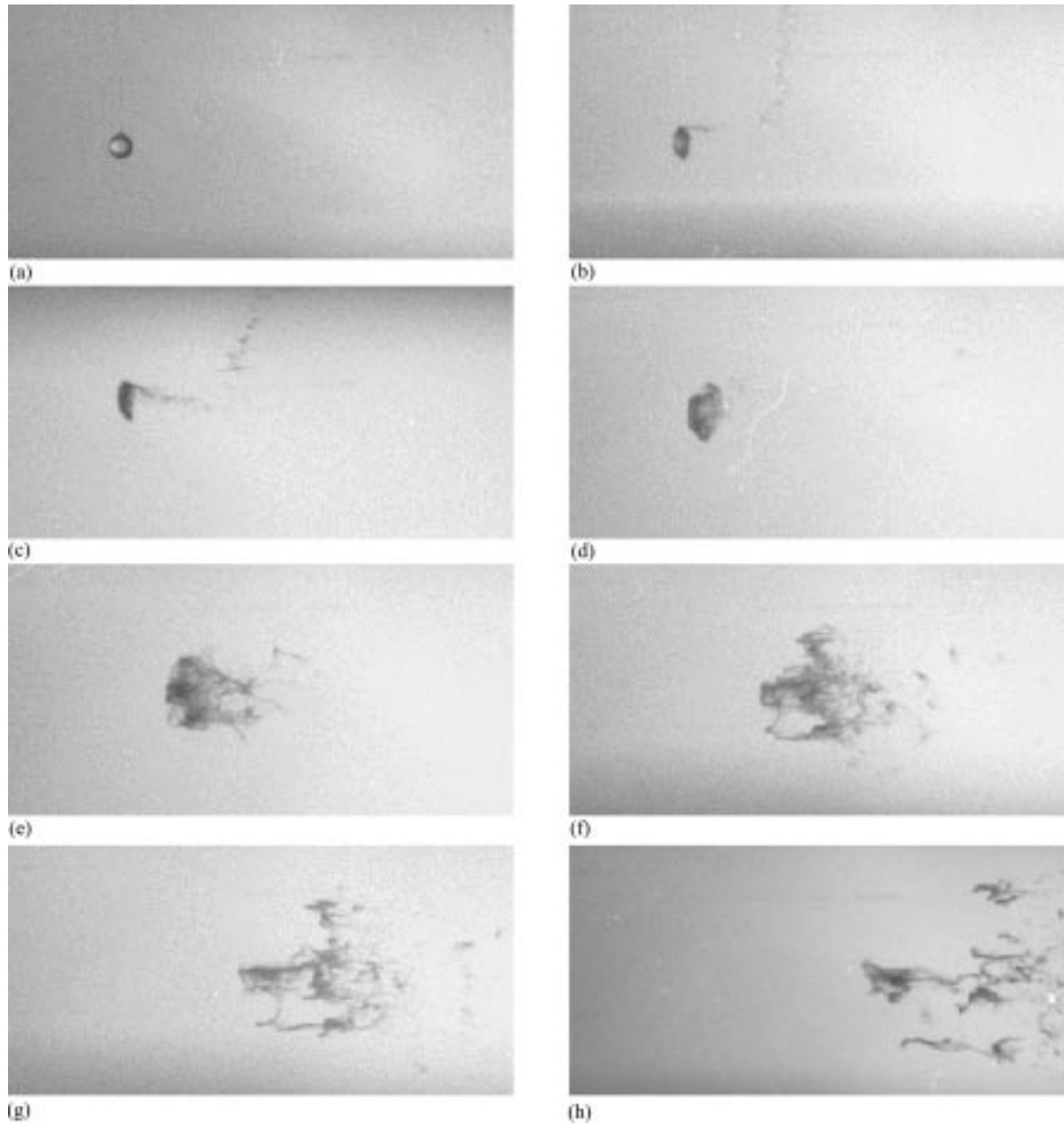


Fig. 7. Stages in the breakup of a drop of 2.6% solution of polystyrene butylacrylate (47025-24) in tributyl phosphate (PSBA/TBP; diameter = 2.2 mm) in the flow behind a Mach 2 shock wave. Air velocity = 435 m/s; dynamic pressure = 152.4 kPa; Weber No. = 31,900. Time (μs): (a) 0, (b) 60, (c) 80, (d) 125, (e) 205, (f) 260, (g) 300, (h) 360.

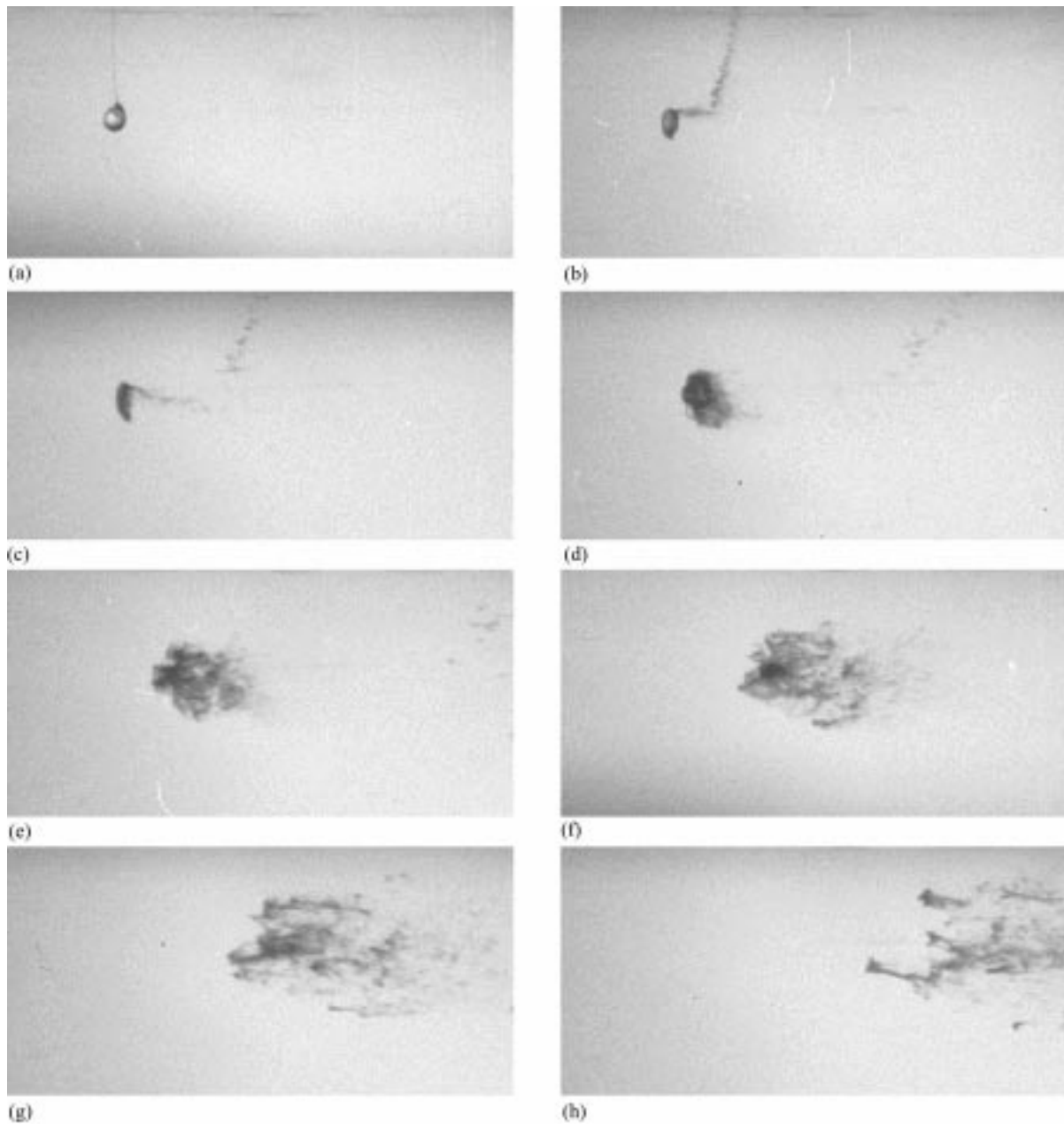


Fig. 8. Stages in the breakup of a drop of 2.6% solution of polystyrene butylacrylate (47025-24) in tributyl phosphate (PSBA/TBP; diameter = 2.2 mm) in the flow behind a Mach 3 shock wave. Air velocity = 736 m/s; dynamic pressure = 513.0 kPa; Weber No. = 107,500. Time (μ s): (a) 0, (b) 30, (c) 50, (d) 80, (e) 105, (f) 135, (g) 160, (h) 200.

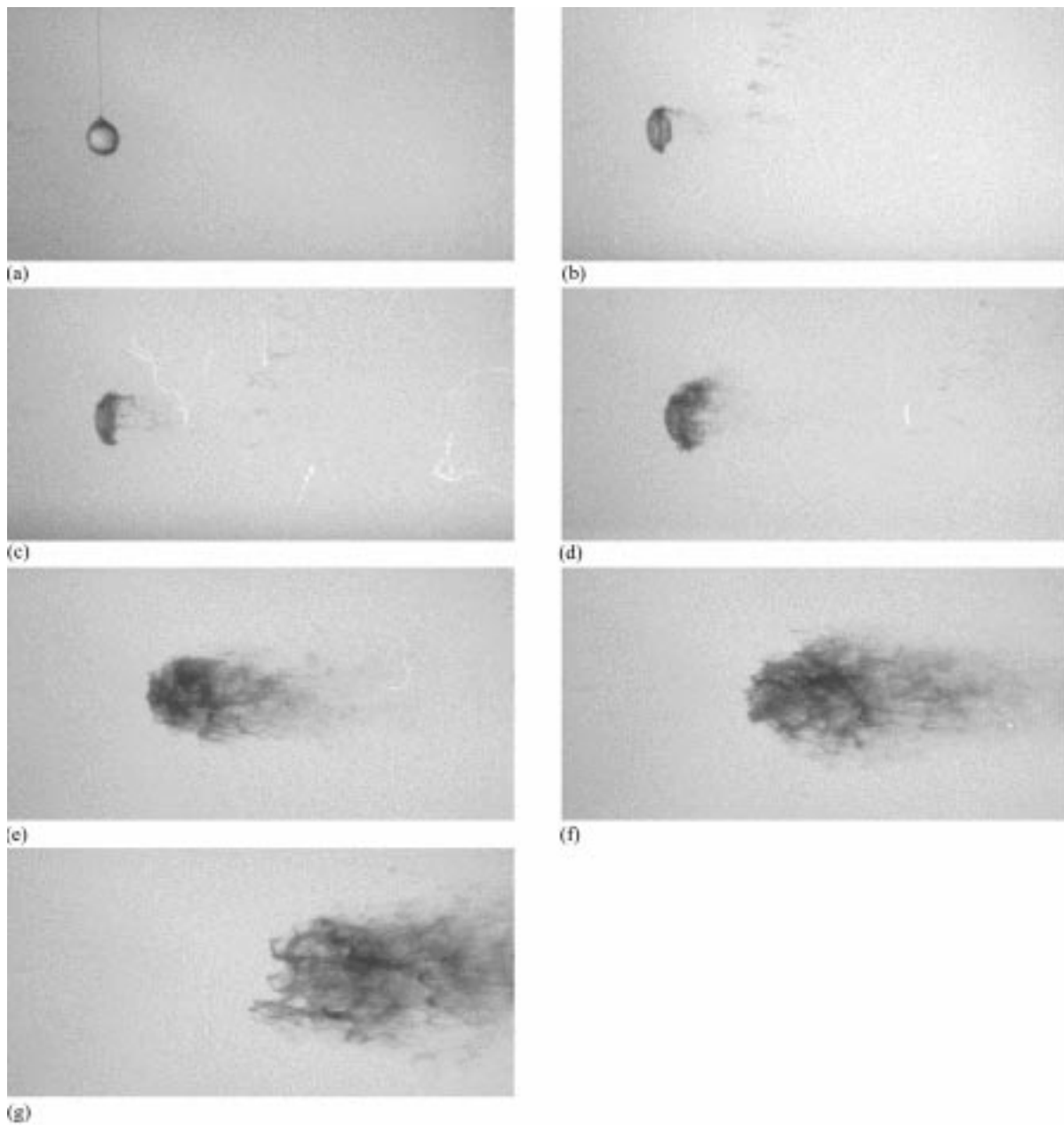


Fig. 9. Stages in the breakup of a drop of 2% aqueous solution of polyacrylamide (Cyanamer N-300LMW; diameter = 3.2 mm) in the flow behind a Mach 3 shock wave. Air velocity = 771 m/s; dynamic pressure = 578.1 kPa; Weber No. = 82,200. Time (μs): (a) 0, (b) 45, (c) 60, (d) 90, (e) 145, (f) 185, (g) 225.

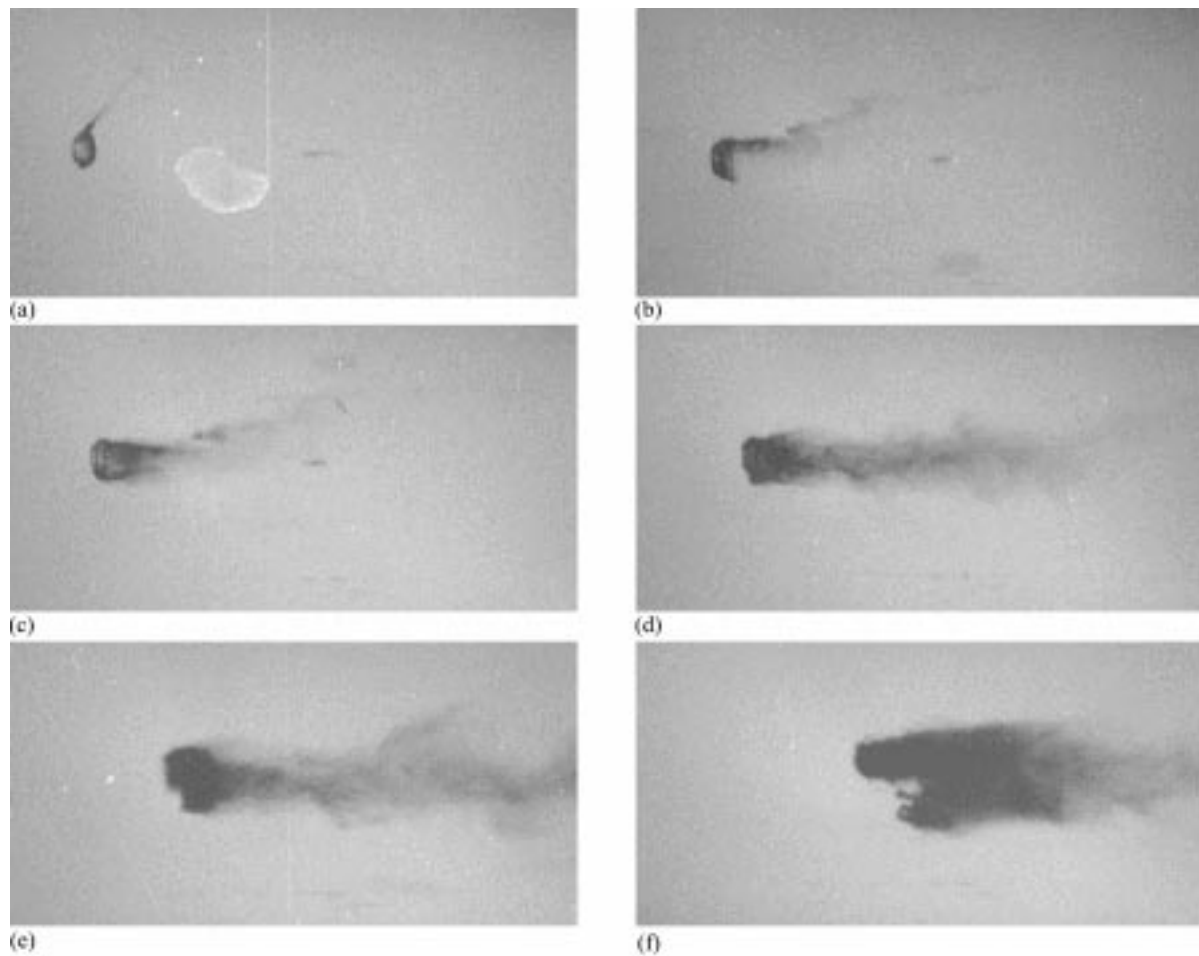


Fig. 10. Example of stripping breakup; a drop of 1 kg/ms silicone oil (diameter = 2.6 mm) in the flow behind a Mach 3 shock wave. Air velocity = 767 m/s; dynamic pressure = 681.0 kPa; Weber No. = 168,600. Time (μ s): (a) 15, (b) 40, (c) 50, (d) 80, (e) 115, (f) 150.

The camera is a Cordin model 377 rotating drum framing camera, operated at 200,000 frames per second. The individual frames are scanned into a workstation and composed into a movie sequence using standard commercial movie-making software.

3. Experiments

The data necessary to specify our experiments are listed in Table 1. The first column identifies the 13 liquids studied; there are eight different silicone oils with viscosities ranging from 0.1 to 10 kg/m s. The Ohnesorge number Oh , the Weber number We and the Reynolds number Re

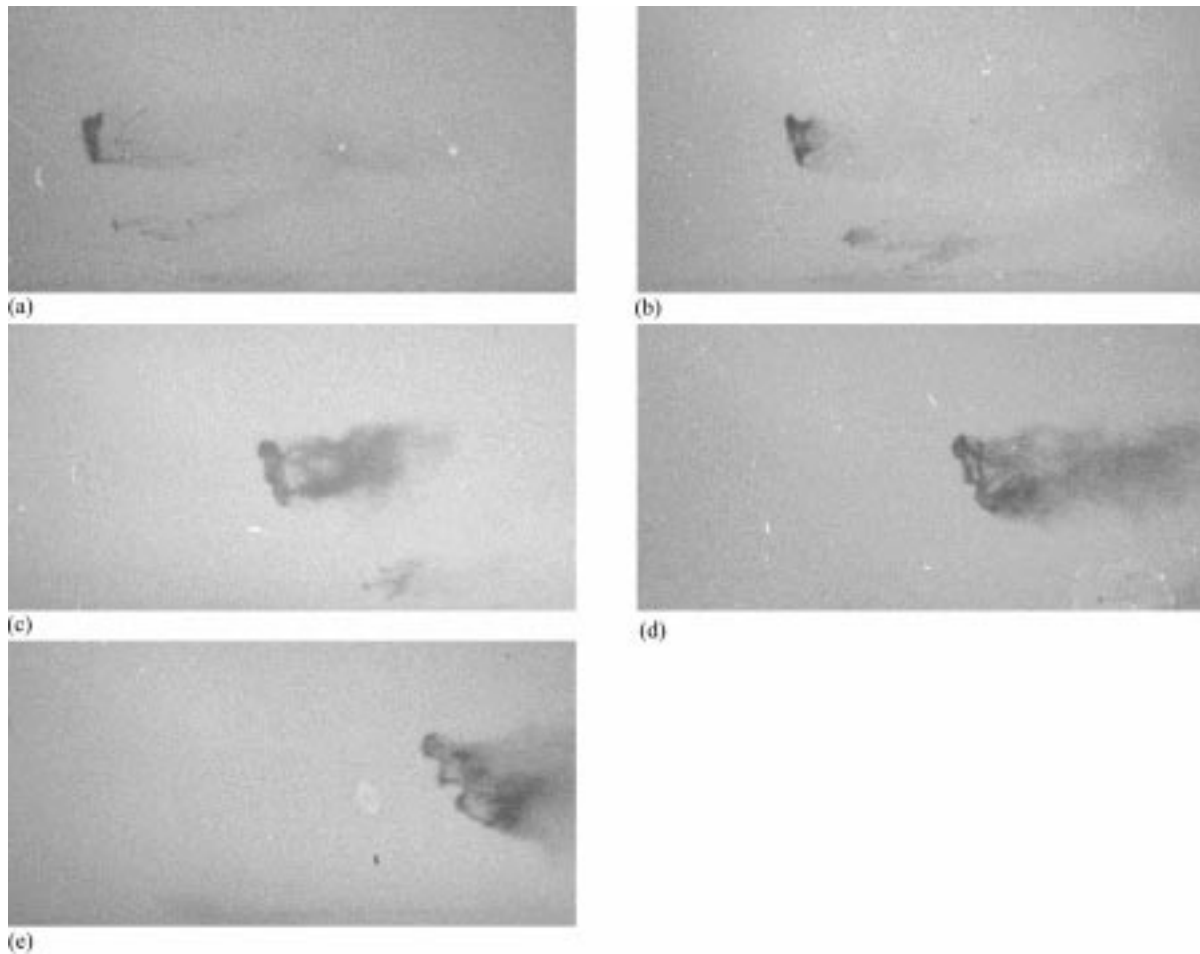


Fig. 11. Example of bag breakup; a drop of 6 kg/ms silicone oil (diameter = 2.5 mm) in the flow behind a Mach 3 shock wave. Air velocity = 761 m/s; dynamic pressure = 666.6 kPa; Weber No. = 158,700. Time (μ s): (a) 265, (b) 290, (c) 320, (d) 340, (e) 365.

$$Oh = \frac{\mu_d}{(\rho_d D \gamma)^{1/2}}, \quad We = \frac{\rho V^2 D}{\gamma}, \quad Re = \frac{VD\rho}{\mu} \quad (1)$$

are defined in terms of the initial drop diameter D , listed in the second column, drop viscosity μ_d , surface tension γ , drop density ρ_d listed in columns 3, 4, 5, respectively, and the free stream values of the velocity V , viscosity μ , and density ρ .

3.1. Time–displacement graphs and accelerations

We have obtained data sets of distance traveled vs. time from many of our experiments. The distance refers to the slowest moving drop fragment; other parts of the fragmenting drop accelerate from rest even more rapidly. Representative graphs are exhibited in Fig. 14; these

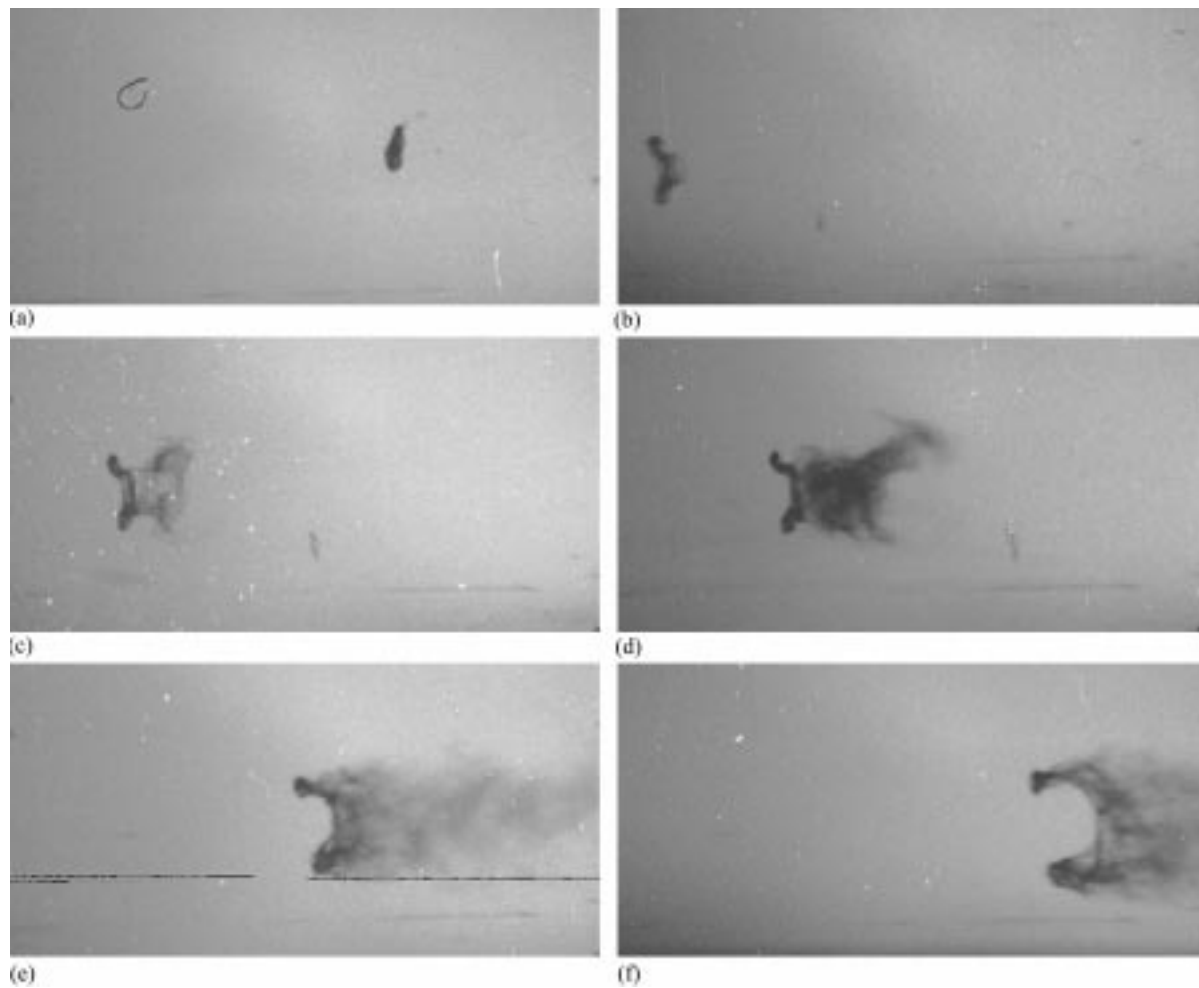


Fig. 12. Example of bag breakup; a drop of 10 kg/ms silicone oil (diameter = 2.6 mm) in the flow behind a Mach 3 shock wave. Air velocity = 754 m/s; dynamic pressure = 652.4 kPa; Weber No. = 161,000. Time (μ s): (a) 360, (b) 375, (c) 390, (d) 405, (e) 425, (f) 455.

graphs are nearly perfect parabolas for the first few hundred microseconds of the motion, and the acceleration 2α can be obtained by curve fitting. It is noteworthy that in these graphs the acceleration is constant, independent of time for small times, and about 10^4 – 10^5 times the acceleration of gravity depending upon the shock wave Mach number. In general, there is a moderate drop-off of acceleration with time over the course of the 400 or 500 μ s it takes to totally fragment the drop.

Table 2 gives the initial accelerations for the drops listed in Table 1 at shock Mach numbers of 2 and 3. The accelerations are an increasing function of the shock Mach number; the dynamic pressure which accelerates the drop increases with the free stream velocity. There appears to be a tendency for the acceleration to decrease with drop size; if we write that the drag on a spherical drop is proportional to the drop diameter squared and the mass to the

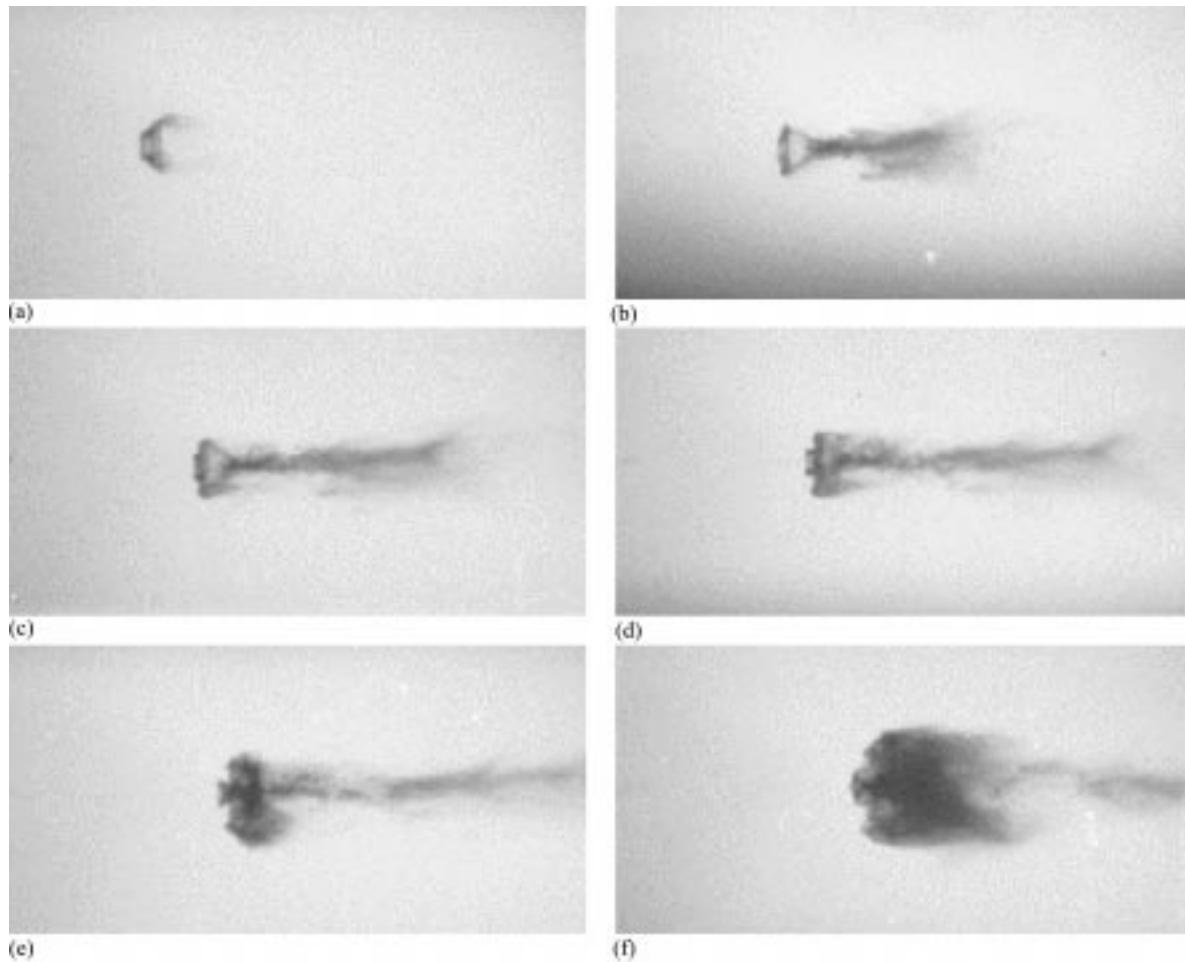


Fig. 13. Example of bag-and-stamen type breakup; a drop of glycerine (diameter = 2.4 mm) in the flow behind a Mach 3 shock wave. Air velocity = 758 m/s; dynamic pressure = 554.0 kPa; Weber No. = 42,200. Time (μ s): (a) 55, (b) 100, (c) 115, (d) 125, (e) 135, (f) 155.

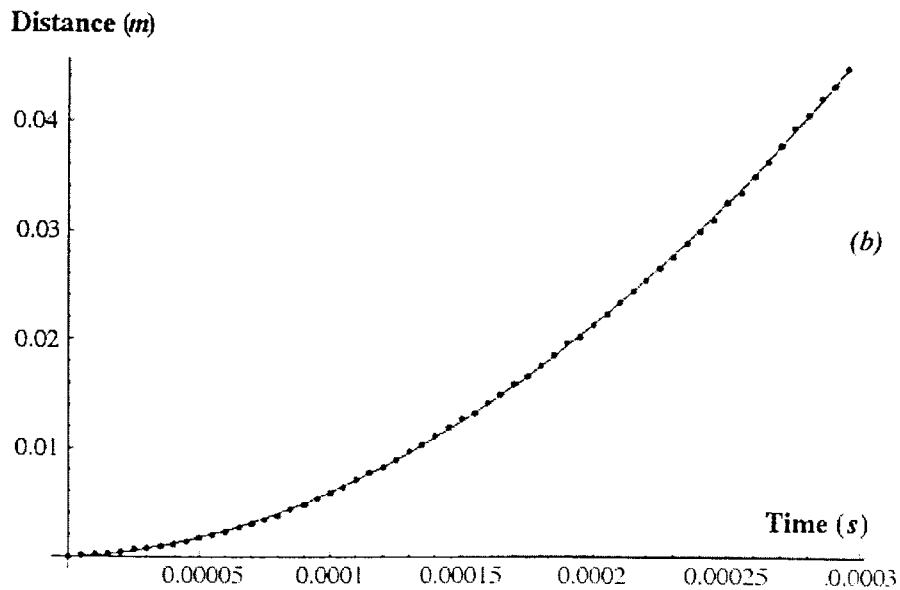
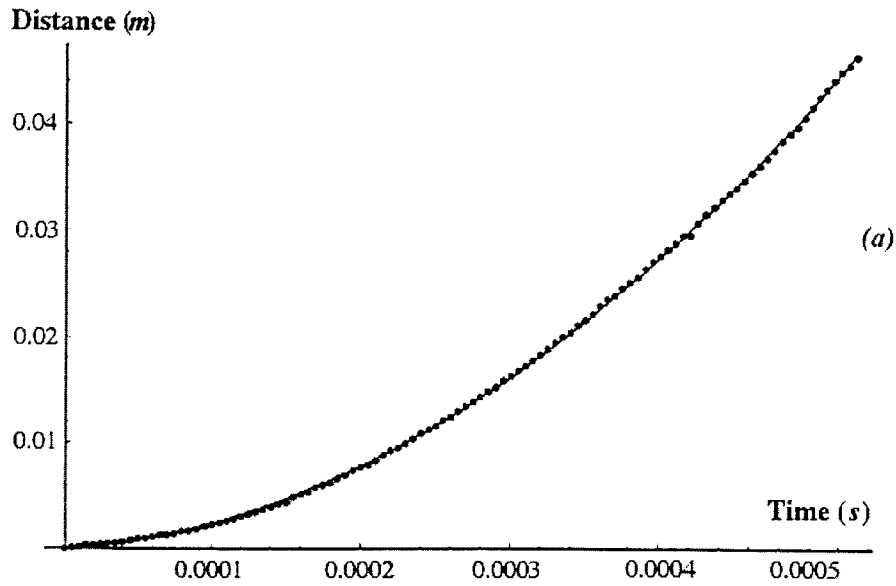
diameter cubed, then the acceleration is proportional to D^{-1} and decreases with increasing D . There is also a tendency for low viscosity drops, like water, to accelerate less rapidly; this reduction is a consequence of the transfer of momentum from the gas stream into deformation of the drop.

4. Description of stages of drop breakup

The permanent record of high speed movies of the breakup of all kinds of liquids at high Weber numbers shares many features with the classifications of breakup at low Weber numbers summarized in the papers of Pilch and Erdman (1987) and Hsiang and Faeth (1992). However, other features in these classifications do not appear in our study, still other features not seen

Table 1
Experimental parameters

Liquid	Liquid properties					Free stream conditions							
	Diameter (mm)	Viscosity (kg/m s)	Surface tension (N/m)	Density (kg/m ³)	Ohnesorge No.	Velocity (m/s)	Density (kg/m ³)	Pressure (kPa)	Dynamic pressure (kPa)	Temperature (K)	Weber No. (10 ³ ×)	Reynolds No. (10 ³ ×)	Shock <i>M</i>
Newtonian													
Water	2.6	0.001	0.07	1000	0.002	431.7	1.696	241.0	158.0	497	11.7	72.1	2.01
Water	2.5	0.001	0.07	1000	0.002	764.3	2.076	468.2	606.4	788	43.3	111.3	3.01
Glycerine	2.3	1.49	0.063	1258	3.5	428.1	1.591	225.0	145.8	494	10.6	59.6	2
Glycerine	2.4	1.49	0.063	1258	3.4	757.9	1.929	431.1	554.0	782	42.2	99.0	2.99
SO 100	2.6	0.1	0.021	969	0.4	435.2	1.866	266.4	176.8	499	43.8	79.7	2.02
SO 100	2.6	0.1	0.021	969	0.4	757.9	2.296	513.2	659.5	782	163.3	127.6	2.99
SO 1000	2.6	1	0.021	969	4.3	438.8	1.876	269.2	180.6	502	44.7	80.6	2.03
SO 1000	2.6	1	0.021	969	4.3	767.4	2.312	523.7	681.0	792	168.6	129.1	3.02
SO 3000	2.6	3	0.021	969	13.0	435.2	1.866	266.4	176.8	499	43.8	79.7	2.02
SO 3000	2.5	3	0.021	969	13.3	754.8	2.290	509.7	652.4	778	155.3	122.3	2.98
SO 3000	2.6	3	0.021	969	13.0	757.9	2.296	513.2	659.5	782	163.3	127.6	2.99
SO 4000	2.47	4	0.021	969	17.8	435.2	1.866	266.4	176.8	499	41.6	75.8	2.02
SO 4000	2.51	4	0.021	969	17.7	754.8	2.290	509.7	652.4	778	156.0	122.8	2.98
SO 4000	2.09	4	0.021	969	19.4	761.1	2.301	516.7	666.6	785	132.7	103.0	3
SO 5000	2.5	5	0.021	969	22.2	761.1	2.301	516.7	666.6	785	158.7	123.2	3
SO 6000	2.6	6	0.021	969	26.1	473.9	1.976	297.3	221.9	526	54.9	88.7	2.13
SO 6000	2.6	6	0.021	969	26.1	754.8	2.290	509.7	652.4	778	161.5	127.2	2.98
SO 6000	2.5	6	0.021	969	26.6	761.1	2.301	516.7	666.6	785	158.7	123.2	3
SO 10000	2.5	10	0.021	969	44.3	438.8	1.876	269.2	180.6	502	43.0	77.5	2.03
SO 10000	2.6	10	0.021	969	43.5	754.8	2.290	509.7	652.4	778	161.5	127.2	2.98
SO 10000	2.5	10	0.021	969	44.3	748.4	2.279	502.8	638.3	771	152.0	121.3	2.96
SO 10000	2.6	10	0.021	969	43.5	1070.3	0.655	222.0	375.0	1186	92.8	40.0	4
Viscoelastic													
2% PO	2.9	35	0.063	990	82.3	431.7	1.776	252.3	165.5	497	15.2	84.2	2.01
2% PO	2.9	35	0.063	990	82.3	424.6	1.756	247.2	158.3	492	14.6	82.5	1.99
2% PO	2.9	35	0.063	990	82.3	754.8	2.061	458.7	587.2	778	54.1	127.6	2.98
2.6% PSBA	2.2	1.13	0.07	900	3.0	435.2	1.609	229.7	152.4	499	9.6	58.2	2.02
2.6% PSBA	2.2	1.13	0.07	900	3.0	735.7	1.896	410.8	513.0	758	32.2	88.2	2.92
2% PAA	3.2	0.96	0.045	990	2.5	770.6	1.947	442.9	578.1	795	82.2	134.0	3.03



	(a)	(b)
Liquid	SO 1000 Silicone Oil	SO 6000 Silicone
Shock Mach No.	2	3
α	1.4627E5	4.8901E5
x_0 (m)	-28.5E-5	-7.91E-5
t_0 (sec)	-3.43E-5	1.21E-5
acc(m/sec ²)	2.92E5	9.78E5

Fig. 14. Distance traveled vs. time. $x - x_0 = \alpha(t - t_0)^2$ where x_0 and t_0 are the extrapolated starting values from the curve fitting technique. The starting values x_0 and t_0 are uncertain within several pixels and 5 μ s.

Table 2

Initial accelerations of drops specified in the data set in Table 1 (see Fig. 14)

Liquid	Viscosity (kg/m s)	Initial acceleration (10^5 m/s ²)		Initial drop diameter (mm)
		$M_s = 3.0$	$M_s = 2.0$	
Silicone oil				
SO 100	0.1	15.8	4.0	2.6
SO 1000	1	11.12	2.92	2.6
SO 3000	3	9.98	3.08	2.6
SO 4000	4	12.06	2.02	2.5
SO 4000	4	11.08	–	2.1
SO 5000	5	8.99	–	2.5
SO 6000	6	9.78	–	2.6
SO 10000	10	7.73	–	2.6
2% Polyox	35	6.48	1.37	2.9
2% Polyacrylamide	0.96	4.92	–	3.2
2.6% PSBA/TBP	1.13	7.28	2.32	2.2
Glycerine	1.49	8.43	4.38	2.4
Water	0.001	6.47	1.52	2.5

by them are captured in our high speed movies, and features which are said to occur only at low Weber numbers in water appear in more viscous drops at Weber numbers orders of magnitude higher. For example, Fig. 11 shows an example of bag-type breakup of 60 kg/m s silicone oil at a Weber number of about 160,000 based on free stream conditions, and Fig. 13 shows an example of breakup of glycerin of a bag-and-stamen type at a Weber number of about 42,000. Many universal structures like nose stripping producing accumulated fluid at the equator (Saturn's rings) and transient lenticular drops, which can be seen clearly in our movies, are not mentioned by Pilch and Erdman or in other works on drop breakup known to us. The surface corrugations seen in their cartoons for $We < 350$ are due to Rayleigh–Taylor instabilities which will be discussed in Section 5.

We shall now describe the sequence of stages of drop breakup at high Weber and Reynolds numbers which can be seen in the movies on our web page (http://www.aem.umn.edu/research/Aerodynamic_Breakup). We have documented these stages with still photos in Figs. 1–13; a fuller understanding of these stages can be obtained by viewing the movies.

The first three stages of breakup numbered below appear to be universal in that they occur in all breakup experiments recorded on our web page; they apply to low and high viscosity liquids and to the viscoelastic liquids of different types that we have studied so far.

4.1. Flattening due to potential flow

In the first 20–30 μ s after the passage of the shock, the flow is not strongly affected by viscosity and can be described as the high speed potential flow of a hot gas over a near sphere of radius r ; the pressure nearly recovers its stagnation value on the back side of the sphere; the sphere is squeezed by these pressures and pulled out at the equator by high speed flow

flattening the sphere. An analysis of this flattening was given by J.M. Burgers in Engel (1958). The analysis is for incompressible flow in the drop with equal pressures p_s at the front and back of the sphere and $p_e < p_s$ at the equator. The outward displacement d at the equator of the drop and perpendicular to the air flow is found to be given for small times t by

$$d = \frac{1}{3} \frac{p_s - p_e}{\rho_d r} t^2 \quad (2)$$

where ρ_d is the drop density and r is its radius. This shows a strong dependence on drop size. Engel (1958) applied Eq. (2) to a later flattening of the drop in which viscosity is important, and found that Eq. (2) predicted the radius correctly but otherwise did not agree with experiments. This points to the necessity of obtaining systematic results from experiments with different size of drops in which viscosity and surface tension are not neglected.

The flattening of the drop at early times is a universal feature apparently independent of drop viscosity or material type at large Weber numbers. The analysis of Rayleigh–Taylor instability of the acceleration of a gas into a liquid at a plane interface is well-suited to a flat drop.

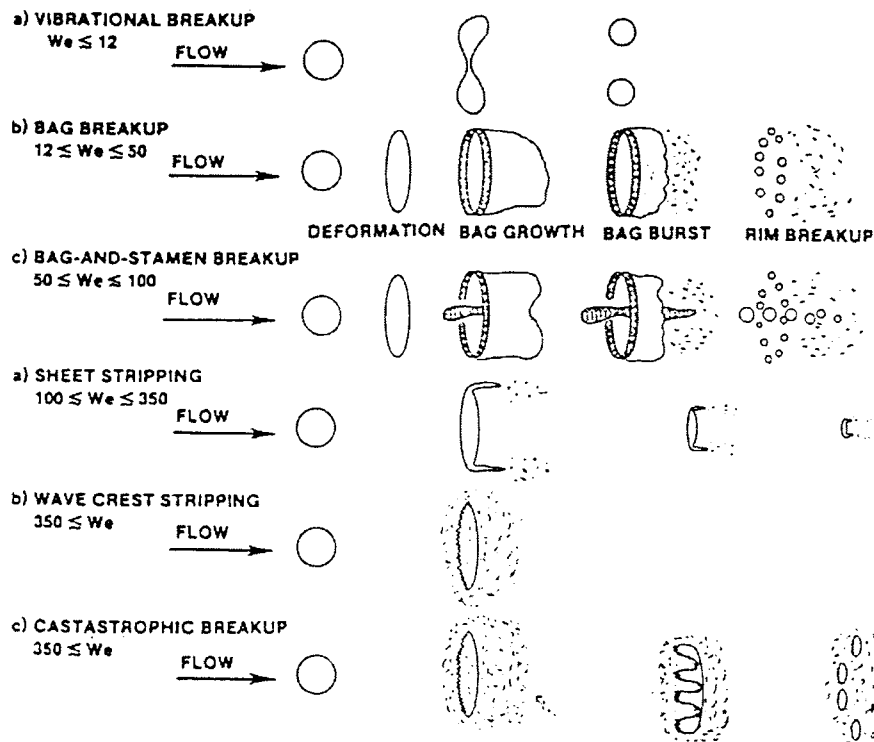


Fig. 15. (Pilch and Erdman, 1987) Cartoon of breakup mechanisms. These mechanisms apply perhaps qualitatively to the breakup of water drops. We know of no experimental evidence for vibrational breakup. The bag and bag-and-stamen breakup can be seen at Weber numbers as large or larger than 42,000 (e.g., Fig. 13), ‘catastrophic’ breakup for high viscosity drops is basically a Rayleigh–Taylor breakup (see Section 5 and Hsiang and Faeth, 1992).

4.2. Radially outward boundary layer flow from the nose of the drop to its equator

This was analyzed by Taylor (1949) in his celebrated Porton Down paper. The analysis was carried out using several severe approximations and the calculations are not in good agreement with experiments. In particular, the flow was assumed to be steady and parallel to the drop surface; the normal component of velocity of the air was neglected and no account was taken of the effects of pervasive corrugations of the interface which are generated by Rayleigh–Taylor instability. Inspection of our movies should convince any doubting reader that the kind of boundary flow studied by Taylor is definitely present in the drop dynamics, and it is involved in an important redistribution of the liquid resulting in change of shape as well as in the stripping of liquid from the drop.

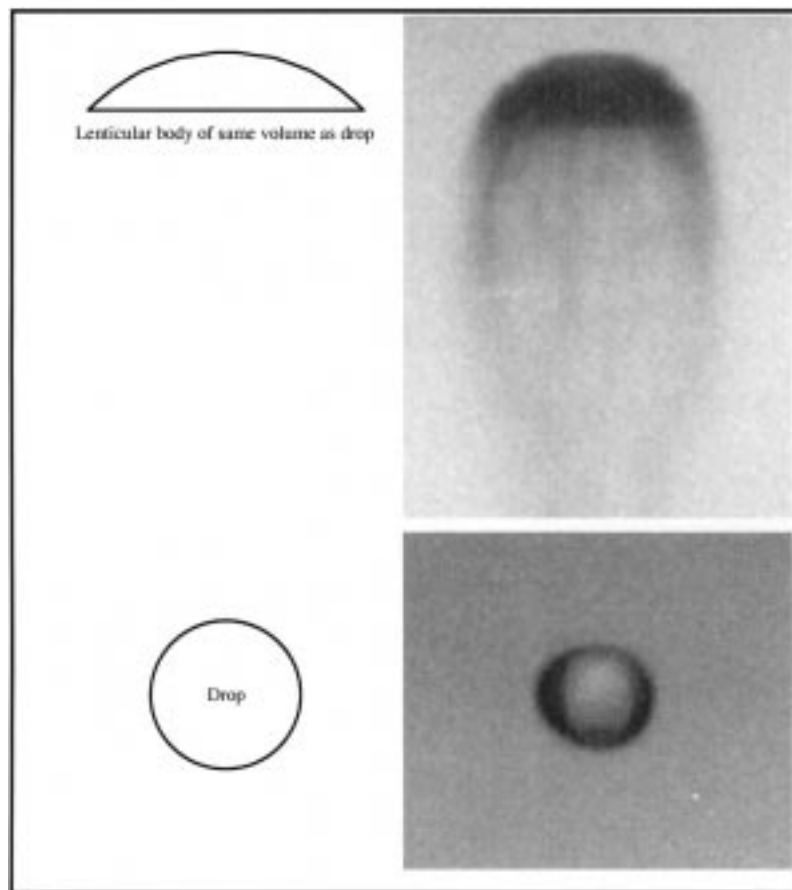


Fig. 16. Comparison of the lenticular shape that Taylor (1949), Fig. 2, predicted a spherical water drop would assume if it did not break up with the lenticular shape of an initially spherical water drop (2.6 mm diameter) 70 μ s after exposure to the flow behind a Mach 2 shock wave in our shock tube.

4.3. Accumulation of liquid at the equator

The liquid driven from the nose of the drop by the high speed airstream accumulates in a thin ring at the equator, like Saturn's rings attached to the drop by a liquid web. The effect, which is not accounted for in the frequently-quoted Pilch and Erdman (1987) classification, reproduced here as Fig. 15, is very dramatic and universal, but the size of the rings and the time interval during which they are present depend upon the liquid and the flow (see, for example, Figs. 3(b) and 4(b) for glycerin, Figs. 5(b) and 6(b) for 2% aqueous polyox, Figs. 7(b) and 8(b) for PSBA/TBP, Fig. 9(b) for 2% polyacrylamide, and Fig. 1(b) for water). The mechanism responsible for the transient accumulation of liquid is not understood and might be best approached by direct numerical simulation.

The following features can be seen in some drops, and not in others.

4.4. Blow-off of liquid from the rings into drops and mist

Capillary instability and generalized cavitation are possible actors in the formation of the clouds, which are formed from the rings. These features are most readily observed in low and not in high viscosity liquids. Compare, for example, Figs. 1 and 2 for water and Fig. 10 for 1 kg/m s silicone oil with Figs. 3 and 4 for glycerin, Figs. 5 and 6 for polyox, and Figs. 7 and 8 for PSBA/TBP.

4.5. Formation of lenticular drops

A lenticular drop has a hemispherical front and flat back (Fig. 16). Some transient structure resembling a lenticular drop always occurs after blow-off.

The lenticular drop forms from the flow of liquid dragged around the nose and accumulated on the equator of the drop. These lenticular drop shapes are most readily observed in low and not in high viscosity liquids (compare Figs. 1 and 2 with Figs. 3 and 4). The lenticular gas bubble rising in a liquid was studied by Davies and Taylor (1950). Taylor (1949) used the same idea to determine the (lenticular) shape which the drop would assume, if it did not disintegrate. The lenticular shape predicted by Taylor's analysis does appear as a transient structure in some cases of low-speed breakup of viscoelastic liquids (see Figs. 5–9), but it always disintegrates, either by flattening at the nose, or by fingering due to Rayleigh–Taylor instability. The paper by Pilch and Erdman (1987) and other literature known to us do not acknowledge these cases.

4.6. Flattening and bursting of very viscous drops

Very viscous Newtonian drops seem not to experience blow off and not give rise to small droplet clouds and mist. They tend to flatten immediately after the effect described in Section 4.3, and travel long distances before breakup (see Figs. 11 and 12, and the movies of 6 and 10 kg/m s silicone oils on our Web page). On the other hand, the viscoelastic liquids with high zero shear viscosity that we have studied break up in much shorter distances.

4.7. Pancake formation and explosive breakup of drops

The very viscous silicone oils finally form a pancake or very flat disk perpendicular to the flow. These flat disks break up explosively, probably as a result of fingers of gas poking through the pancake. This breakup resembles ‘bag breakup’ in which the air ‘inflates’ a balloon, which ultimately bursts (see Figs. 11 and 12 for the breakup of 6 and 10 kg/m s silicone oils); this kind of breakup, which has been discussed, for example, by Pilch and Erdman (1987), generally occurs at much lower Weber numbers. In fact, it takes so long to break up a very viscous drop that the drop has already accelerated to 40% or more of the free stream value so that the slip velocity is perhaps at a low value compatible with bag breakup.

4.8. Thickened liquids

Thickened liquids give rise to basically the same pre-breakup dynamics as Newtonian drops; the drop flattens, fluid is driven to the equator and sheets of liquid are dragged backwards to form lenticular shapes. However, the breakup of liquids thickened with high molecular weight polymers differs from the breakup of the neat non-thickened Newtonian liquid; the neat liquid gives rise to breakup of the type already discussed but thickened liquid is fragmented into threads which are the dominant structure seen in all photographs and in our movies (see Figs. 5–9). Even threads of these liquids can be seen to maintain their integrity in high Mach number flow; it is known that these threads do not undergo capillary instabilities leading to small drops.

5. Stability

Rayleigh–Taylor instabilities (Taylor, 1950) always play a role in drop breakup. Rayleigh showed that a heavy fluid over a light fluid is unstable, as common experience dictates. He treated the stability of heavy fluid over light fluid without viscosity, and he found that a disturbance of the flat free surface grows exponentially like $\exp(nt)$ where

$$n = \left\{ \frac{kg(\rho_2 - \rho_1)}{\rho_1 + \rho_2} \right\}^{1/2} \quad (3)$$

where ρ_2 is the density of the heavy fluid, ρ_1 is the density of the light fluid, g is the acceleration of gravity and $k = 2\pi/\lambda$ is the wave number and λ is the wave length. The instability described by Eq. (3) is catastrophic since the growth rate n tends to infinity, at any fixed time, no matter how small, as the wave length tends to zero. The solutions are unstable to short waves even at the earliest times. Such kinds of disastrous instabilities are called ‘Hadamard unstable’ and the initial value problems associated with these instabilities are said to be ‘ill posed’ (Joseph and Saut, 1990). Ill-posed problems are disasters for numerical simulations. Because such problems are unstable to ever shorter waves, the finer the mesh, the worse the result.

Nature will not allow such a singular instability; for example, neglected effects like viscosity and surface tension will enter the physics strongly at the shortest wave lengths. These effects have been taken into account in the study of Rayleigh–Taylor instability by Harrison (1908) and in the celebrated treatise of Chandrasekhar (1961). Surface tension eliminates the instability of the short waves; there is a finite wave length depending strongly on viscosity, as well as surface tension for which the growth rate n is maximum. This is the wave length that should occur in a real physical problem and would determine the wave length on the corrugated fronts of breaking drops in a high speed air flow.

Taylor (1950) extended Rayleigh's inviscid analysis to the case where a constant acceleration of the superposed fluids other than gravity is taken into account. Assuming a constant value for the acceleration, Taylor (1950) showed that when two superposed fluids of different densities are accelerated in a direction perpendicular to their interface, this surface is unstable if the acceleration is directed from the lighter to the heavier fluid. The Taylor instability depends strongly on the value of the acceleration a ; for example, if g in Eq. (3) is replaced by $a = 10^4g$, the growth rate n is increased by a factor of 100. 10^4g to 10^5g are representative values of the acceleration of drops in our shock tube; moreover the acceleration is nearly constant for all liquid drops at a given shock Mach number (see Table 2). A similar observation was made by Engel (1958). Since the acceleration is perpendicular to the air–liquid interface and directed from gas to liquid, the accelerating liquid drop is unstable and is prey to the characteristic short wave corrugation associated with this instability.

Lewis (1950) has shown experimentally that a layer of water driven by compressed air is unstable and that small disturbances, introduced at the air–water interface, grow so that it appears as though fingers of air move through the water layer. Lewis (1950) finds agreement with his experiments when the viscosity of the liquid is small. The peaks of water in his experiments are sharp, but the match between Taylor's theory and the Lewis experiment is not perfect because the regularizing effects of surface tension were neglected. When the finger of air reaches the opposite surface of the water layer in the experiments, thin bubbles of liquid blow out ahead of them. These bubbles are like the 'bag breakup' shown in Fig. 16. The explosive breakup of pancakes of high viscosity silicone oil at Mach 3 (Figs. 11 and 12) and Mach 4 (not shown; similar to Fig. 12) appears to be associated with this same kind of explosive break through the penetration of fingers of air.

The corrugations at the front of an unstable drop are driven toward the drop equator by shear flow of gas coming from the high pressure stagnation point. This shear flow may also be subject to an instability of the Kelvin–Helmholz type. Since the tangential velocity is zero at the stagnation point and small near the stagnation point, the Kelvin–Helmholz instability may not interact too strongly with the Rayleigh–Taylor instability.

Some details of the corrugations on the front of breaking drops can be predicted by mathematical analysis of the foregoing instabilities, but the effects of viscosity and surface tension must be taken into account.

A thorough explanation and analysis of the Rayleigh–Taylor instability can be found in Chapter X of the treatise by Chandrasekhar. In Chandrasekhar's analysis, the two fluids are separated by an interface $z = h(x,y,t)$ which perturbs the plane $z = 0$. The Navier–Stokes equations for the perturbation velocity \mathbf{u} , perturbation pressure p are solved above and below the plane $z = 0$. Gravity points down against the direction of z increasing. It is assumed that

the heavy fluid is above the light fluid, or that the light fluid is accelerated into the heavy fluid above; (the drop is the heavy fluid and the gas flowing into and around it, is the light fluid). At the flat interface at $z = 0$, the linearized kinematic equation is

$$\omega = \frac{\partial h}{\partial t} \quad (4)$$

where

$$[[\omega]] = \omega_2 - \omega_1 \quad (5)$$

is the jump in the normal (z component) of velocity (ω_2 is in $z > 0$, ω_1 in $z < 0$). For the viscous case the jump in the tangential velocity is also zero

$$[[\omega]] = [[u]] = [[v]] = 0 \quad (6)$$

where u is in the x direction and v in the y direction. Since Eq. (6) holds for all x and y for $z = 0$, we may deduce that

$$\left[\left| \frac{\partial u}{\partial x} + \frac{\partial v}{\partial y} \right| \right] = - \left[\left| \frac{\partial \omega}{\partial z} \right| \right] = 0 \quad (7)$$

The continuity of the shear stress is expressed by

$$\left[\left| \mu \left(\frac{\partial u}{\partial z} + \frac{\partial \omega}{\partial x} \right) \right| \right] = 0$$

$$\left[\left| \mu \left(\frac{\partial v}{\partial z} + \frac{\partial \omega}{\partial y} \right) \right| \right] = 0 \quad (8)$$

where μ is the viscosity.

The balance of normal stress is given by

$$-[[p]] + 2 \left[\left| \mu \frac{\partial \omega}{\partial z} \right| \right] = -\gamma \left(\frac{\partial^2}{\partial x^2} + \frac{\partial^2}{\partial y^2} \right) h \quad (9)$$

where γ is the surface tension. We may remove the hydrostatic pressure from the z equation of motion by introducing the dynamic pressure

$$\pi = p + \rho gh$$

hence,

$$[[\pi]] = gh[[\rho]] + 2 \left[\left| \mu \frac{\partial \omega}{\partial z} \right| \right] + \gamma \left(\frac{\partial^2}{\partial x^2} + \frac{\partial^2}{\partial y^2} \right) h \quad (10)$$

After introducing normal modes proportional to

$$f(z)e^{nt+ik_x x+ik_y y}, \quad k^2 = k_x^2 + k_y^2 \tag{11}$$

where $f(z)$ is an amplitude function for π, u, v and h which may be eliminated to find Eq. (40) on page 433 of Chandrasekhar (1961):

$$\begin{aligned} & \left[\left| \left\{ \rho - \frac{\mu}{n} \left(\frac{d^2}{dz^2} - k^2 \right) \right\} \frac{d\omega}{dz} - \frac{1}{n} \left\{ \left(\frac{d^2}{dz^2} + k^2 \right) \omega \right\} \frac{d\mu}{dz} \right| \right] \\ & = -\frac{k^2}{n^2} \{ g[|\rho|] - k^2 \gamma \} \omega - \frac{2k^2}{n} \left[\left| \mu \frac{d\omega}{dz} \right| \right] \end{aligned} \tag{12}$$

For the present problem, for which the unperturbed states above and below $z = 0$ are uniform, $d\mu/dz = 0$ and using Eq. (7)

$$\left[\left| \mu \frac{d\omega}{dz} \right| \right] = [|\mu|] \frac{d\omega}{dz} \tag{13}$$

The entire problem is resolved by

$$\begin{aligned} \omega_1 &= A_1 e^{kz} + B_1 e^{q_1 z} \quad (z < 0) \\ \omega_2 &= A_2 e^{-kz} + B_2 e^{-q_2 z} \quad (z > 0) \end{aligned} \tag{14}$$

where

$$\begin{aligned} q_1 &= \sqrt{k^2 + n/\nu_1} \quad \text{and} \quad q_2 = \sqrt{k^2 + n/\nu_2} \\ \nu_1 &= \mu_1/\rho_1, \quad \nu_2 = \mu_2/\rho_2 \end{aligned} \tag{15}$$

provided that Chandrasekhar’s equation (113) below is satisfied

$$\begin{aligned} & - \left\{ \frac{gk}{n^2} \left[(\alpha_1 - \alpha_2) + \frac{k^2 \gamma}{g(\rho_1 + \rho_2)} \right] + 1 \right\} (\alpha_2 q_1 + \alpha_1 q_2 - k) - 4k\alpha_1 \alpha_2 + \frac{4k^2}{n} (\alpha_1 \nu_1 - \alpha_2 \nu_2) \\ & \times \{ (\alpha_2 q_1 - \alpha_1 q_2) + k(\alpha_1 - \alpha_2) \} + \frac{4k^3}{n^2} (\alpha_1 \nu_1 - \alpha_2 \nu_2)^2 (q_1 - k)(q_2 - k) \\ & = 0 \end{aligned} \tag{16}$$

where

$$\alpha_1 = \frac{\rho_1}{\rho_1 + \rho_2}, \quad \alpha_2 = \frac{\rho_2}{\rho_1 + \rho_2}, \quad \alpha_1 + \alpha_2 = 1$$

In our problem the light fluid is gas; with only a very small error we may treat this as a vacuum. Hence, we put

$$\rho_1 = \alpha_1 = 0, \quad \alpha_2 = 1$$

$$q_1 \rightarrow k, \quad \alpha_2 q_1 + \alpha_1 q_2 - k \rightarrow q_1 - k$$

$$(\alpha_2 q_1 - \alpha_1 q_2) + k(\alpha_1 - \alpha_2) \rightarrow q_1 - k \quad (17)$$

and, after factoring $q_1 - k$ in Eq. (16) we get

$$1 - \frac{gk}{n^2} = -\frac{k^3 \gamma}{n^2 \rho_2} - \frac{4k^2 \mu_2}{n \rho_2} + \frac{4k^3 \mu_2^2}{n^2 \rho_2^2} (q_2 - k) \quad (18)$$

The Rayleigh–Taylor instability may also be analyzed as a viscous potential flow (Joseph, 1994). In this approach, the perturbation velocity is given by a potential

$$\mathbf{u} = \nabla \phi \quad (19)$$

and the Navier–Stokes equations are reduced to an identity provided that the pressure is given by Bernoulli's equation

$$p + \rho \frac{\partial \phi}{\partial t} + \rho g z = -\frac{\rho}{2} |\nabla \phi|^2 \quad (20)$$

In this linearization used to study instability, the second term on the right side of Eq. (20) is put to zero. The interface condition requires continuity of tangential velocities, Eqs. (6) and (7), and the continuity of shear stress, Eq. (8), cannot be enforced in viscous potential flow. The pressure in the normal stress condition (9) is eliminated using Eq. (20); this gives rise to

$$\left[|\rho \frac{\partial \phi}{\partial t}| \right] + gh[|\rho|] + 2 \left[|\mu \frac{\partial \omega}{\partial z}| \right] + \gamma \left(\frac{\partial^2}{\partial x^2} + \frac{\partial^2}{\partial y^2} \right) h = 0 \quad (21)$$

After introducing normal modes, writing Eq. (4) as $nh = \omega$, we get

$$n[|\rho \phi|] + \frac{\omega}{n}[|\rho|]g + 2 \left[|\mu \frac{\partial \omega}{\partial z}| \right] - \frac{\gamma k^2}{n} \omega = 0 \quad (22)$$

For viscous potential flow, $\nabla^2 \phi = 0$ everywhere and Eq. (14) holds with $B_1 = B_2 = 0$ and

$$\frac{d\omega}{dz} = \frac{d^2 \phi}{dz^2} = k^2 \phi \quad (23)$$

After writing $[|\rho \phi|] = (1/k^2)[|\rho d\omega/dz|]$ in Eq. (22), we may verify that Eqs. (12) and (22) are identical when Eq. (12) is evaluated for viscous potential flow. Further evaluation of Eq. (22) with normal modes give rise to the dispersion relation

$$1 = \frac{k \rho_2 - \rho_1}{n^2 \rho_2 + \rho_1} g - \frac{k^3 \gamma}{n^2 (\rho_2 + \rho_1)} - \frac{2k^2 \mu_2 + \mu_1}{n \rho_2 + \rho_1} \quad (24)$$

Eq. (24) may be solved for the growth rate

$$n = -k^2 \frac{\mu_2 + \mu_1}{\rho_2 + \rho_1} \pm \left[k \frac{\rho_2 - \rho_1}{\rho_2 + \rho_1} g - \frac{k^3 \gamma}{\rho_2 + \rho_1} + k^4 \left(\frac{\mu_2 + \mu_1}{\rho_2 + \rho_1} \right)^2 \right]^{1/2} \quad (25)$$

If the quantity under the root is negative, then the real part is negative and the interface is stable. For instability it is sufficient that

$$\sqrt{k \frac{\rho_2 - \rho_1}{\rho_2 + \rho_1} g + k^4 \left(\frac{\mu_2 + \mu_1}{\rho_2 + \rho_1} \right)^2} - \frac{k^3 \gamma}{\rho_2 + \rho_1} > k^2 \frac{\mu_2 + \mu_1}{\rho_2 + \rho_1} \quad (26)$$

The border of instability $n = 0$ for $k = k_c$ is given by

$$k_c = \sqrt{\frac{(\rho_2 - \rho_1)g}{\gamma}} \quad (27)$$

independent of viscosity.

The quantity of greatest interest is the wave number k for which n is largest ($dn/dk = 0$) and that value of n (see Figs. 17 and 18 and Table 3).

Evaluation of the growth rate formula (25) for the conditions (17) close to our experiments gives

$$n = -\frac{k^2 \mu_2}{\rho_2} \pm \sqrt{kg - \frac{k^3 \gamma}{\rho_2} + \frac{k^4 \mu_2^2}{\rho_2^2}} \quad (28)$$

It is of interest to compare the growth rate formula (28) for viscous potential flow with the growth rate formula (18) for fully viscous flow. These two formulas give almost exactly the same growth rate when

$$q_2 - k = k \sqrt{1 + \frac{n\rho_2}{\mu_2 k^2}} - k \cong \frac{n\rho_2}{2\mu_2 k} \quad (29)$$

and

$$\frac{n\rho_2}{2\mu_2 k} \ll 1 \quad (30)$$

To evaluate the formulas for Rayleigh–Taylor instability for our experiments, we must

$$\text{replace } g \text{ with } a \quad (31)$$

with values of a taken from Table 2. Eq. (27) then implies that

$$k_c = \frac{2\pi}{\lambda_c} = \sqrt{\frac{\rho_2 a}{\gamma}} \quad (32)$$

and waves with length

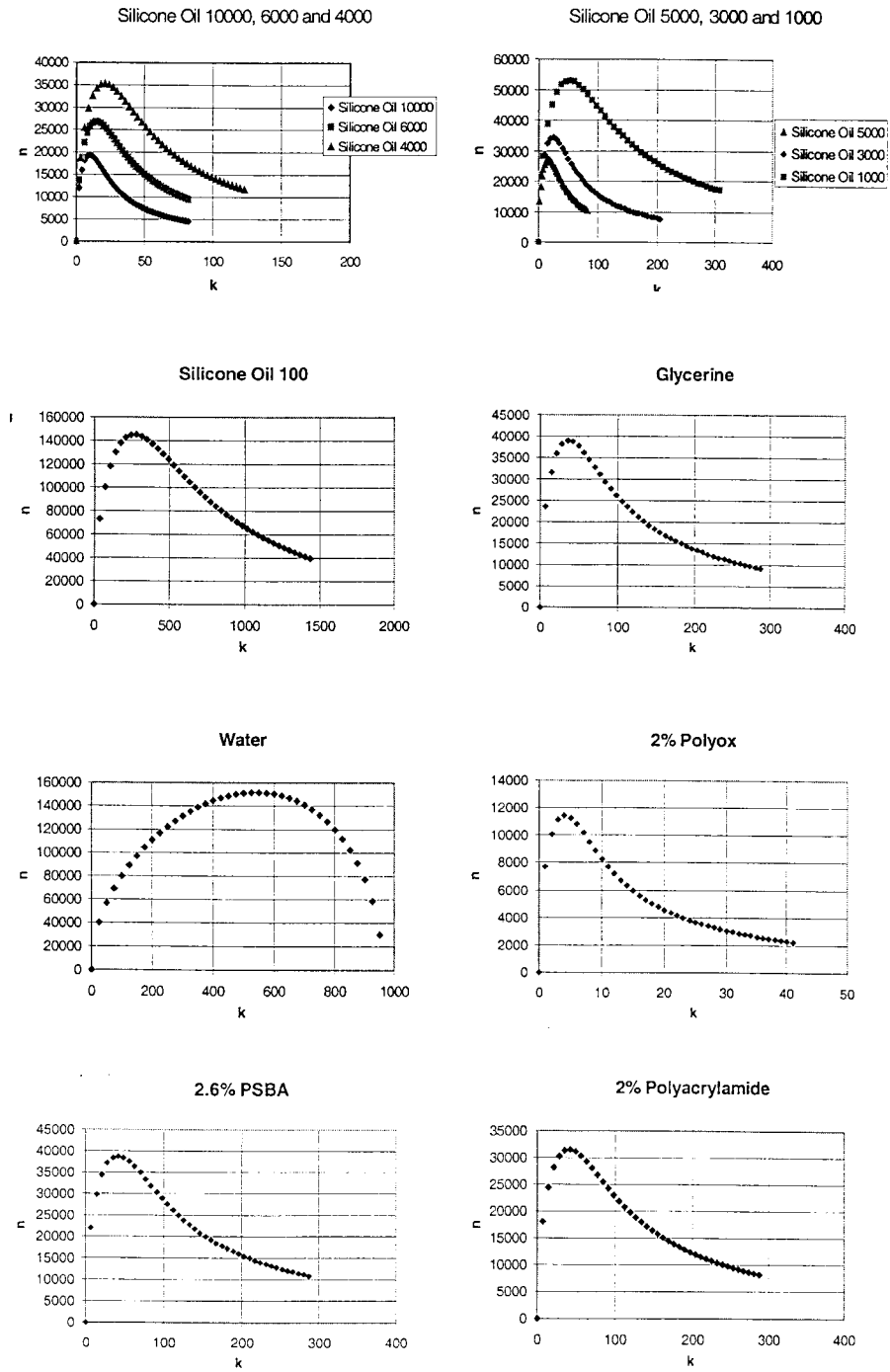


Fig. 17. n (s⁻¹) vs. k (cm⁻¹) for viscous potential flow; shock Mach No. = 3.

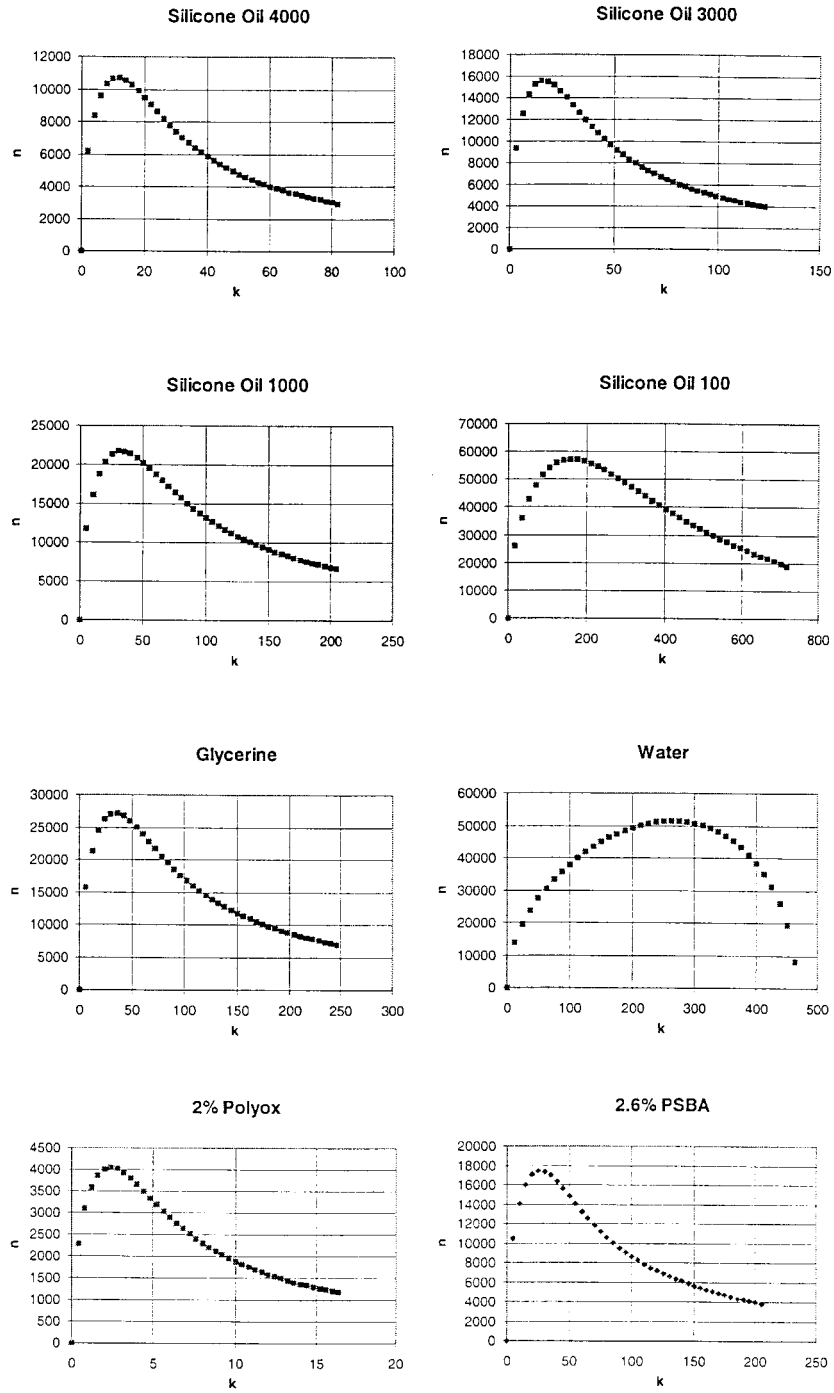


Fig. 18. n (s^{-1}) vs. k (cm^{-1}) for viscous potential flow; shock Mach No. = 2.

Table 3

Values of the wave number, wave length, and growth rate of the most dangerous wave for the experimental conditions given in Tables 1 and 2

Liquid	Viscosity (kg/m s)	Fully viscous			Viscous potential		
		n (s ⁻¹)	k (cm ⁻¹)	λ (mm)	n (s ⁻¹)	k (cm ⁻¹)	λ (mm)
$M_s = 3$							
SO 10000	10	17,790	9.5	6.61	19,342	9.7	6.48
SO 6000	6	24,673	14.45	4.35	26,827	14.7	4.27
SO 5000	5	24,787	15.86	3.96	26,951	16.15	3.89
SO 4000	4	32,550	20.3	3.10	35,312	20.7	3.04
SO 3000	3	31,507	23.08	2.72	34,257	23.5	2.67
SO 1000	1	48,769	49.68	1.26	53,088	50.65	1.24
SO 100	0.1	132,198	253.2	0.25	143,699	259	0.24
Glycerine	1.49	38,760	41.3	1.52	42,141	42.1	1.49
2% PO	35	10,492	3.95	15.91	11,406	3.95	15.91
2.6% PSBA	1.13	34,460	37.8	1.66	37,467	38.5	1.63
2% PAA	0.96	28,927	39.4	1.59	31,451	40.15	1.56
Water	0.001	149,632	531.95	0.12	151,758	540.8	0.12
$M_s = 2$							
SO 4000	4	9868	11.2	5.61	10,729	11.4	5.51
SO 3000	3	14,388	15.6	4.03	15,644	15.9	3.95
SO 1000	1	20,018	31.8	1.98	21,765	32.4	1.94
SO 100	0.1	52,726	158	0.40	57,304	161.9	0.39
Glycerine	1.49	25,046	33.2	1.89	27,231	33.8	1.86
2% PO	35	3723	2.35	26.74	4048	2.4	26.18
2.6% PSBA	1.13	16,070	25.75	2.44	17,472	26.25	2.39
Water	0.001	50,971	260.9	0.24	51,507	264.2	0.24

$$\lambda < \lambda_c = 2\pi \sqrt{\frac{\gamma}{\rho_2 a}} \quad (33)$$

are stable. Taking liberties with Eq. (33), we identify $\lambda = D$ where D is the diameter of drops with acceleration a that cannot be fragmented by Rayleigh–Taylor instability. Applying this to our experiments (Tables 1 and 2), we get D between

$$23 \text{ and } 65 \mu\text{m} \quad \text{for } M_s = 3 \quad (34)$$

$$46 \text{ and } 135 \mu\text{m} \quad \text{for } M_s = 2 \quad (35)$$

Turning next to the computation of the length and growth rate of the most dangerous wave, we computed n vs. k for fully viscous flow, Eq. (18), and viscous potential flow, Eq. (28). The dispersion relations for viscous potential flow, using data from Tables 1 and 2, are plotted in Figs. 17 and 18 for shock Mach numbers of 3 and 2, respectively. The values of the wave number, wave length and growth rate of the most dangerous wave are summarized in Table 3, where we have compared values from viscous potential flow to fully viscous flow. The very small differences shown in this comparison show that the essential effect of viscosity is

associated with the action of the viscous component of the normal stress; the continuity of the tangential component of the stress and velocity can be neglected with only small errors. This kind of dynamics is associated with the fact that vorticity boundary layers at water/air interfaces are very weak and viscous potential flow will not work well at liquid/liquid interfaces or at fluid/solid boundaries. Two other notable successes of viscous potential flow are the rising air bubble (Levich, 1949) and the Rayleigh–Plesset air bubble (Plesset and Prosperetti, 1977).

It is apparent from Table 3 that the most dangerous wave is a strong function of viscosity; the length of this wave increases and the growth rate decreases as the viscosity increases.

6. Comparison of theory and experiment

We used image enhancing software to compare photos from our movies with the stability theory presented in Section 5. No special choice was made in selecting the frames for the comparisons other than choosing ones from the early part of the motion that were well-focused. The wave-like structure can be identified much more easily on the computer screen than in the images reproduced in Figs. 19–22. In Fig. 19, we have compared the predicted wave length with waves enhanced on a water drop at $M = 2$ and 3 with the parameters given by Tables 2 and 3. The tick marks on the photos identify wave troughs so that the predicted distance between tick marks is the length of an unstable wave. The same kind of comparison is given in Fig. 20 for the 0.1 kg/m s silicone oil, in Fig. 21 for the 1 kg/m s silicone oil and in Fig. 22 for glycerine.

The agreements between theory and experiment exhibited in Figs. 19–22 may extend to the higher viscosity drops in our database; the lengths of the most unstable wave for these drops are greater than the diameter of the drop. These drop diameters are larger than the values (34) and (35), hence, shorter waves than the ones listed in Table 3 are still unstable. These shorter waves have much smaller growth rates and, hence, the growth of the amplitude e^{nt} of these waves is very retarded. The retardation of the instability of unstable waves which is predicted by theory is realized in experiments; the larger the viscosity the larger is the length of time it takes for the drop to break. Eventually they do break and the breakup looks like a bag breakup (see Figs. 11 and 12).

The connection between growth rates and breakup time is examined in a different way in Table 4 and Fig. 23. The open symbols in that figure are experimental breakup times and the corresponding solid symbols represent a theoretical prediction of the time \hat{t}_b to breakup of the fastest growing disturbance associated with the most dangerous wave.

We may define a theoretical ‘break-up’ time as the time \hat{t}_b taken for the initial amplitude A_0 of an unstable disturbance $A(t) = A_0 e^{nt}$ to grow to M times its initial value; thus

$$M = \frac{A(\hat{t}_b)}{A_0} = e^{n\hat{t}_b} \quad \text{and} \quad \hat{t}_b = \frac{1}{n} \ln M \quad (36)$$

In Table 4 and Fig. 23, we compare this theoretical value (for $M = 10$) with the time taken to ‘blow off’ the liquid accumulated at the equator of the drop. This ‘blow-off’ time is not difficult

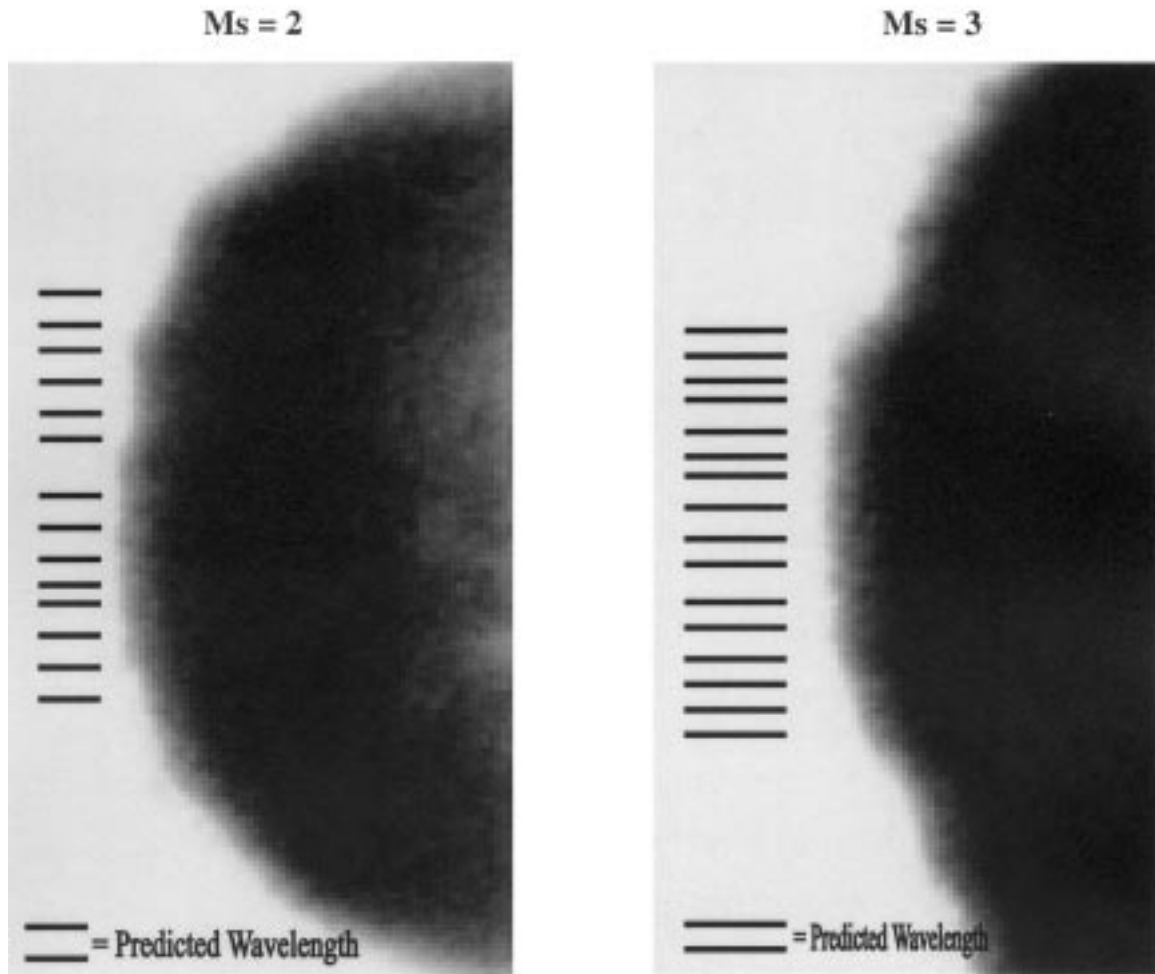


Fig. 19. Rayleigh–Taylor waves in water. The tick marks on the photographs locate wave troughs.

to identify with small error in experiments with mobile liquids; for more viscous liquids the wave length of maximum growth is larger than the drop diameter and bag break-up with smaller growth rates is observed.

7. Remarks about the mechanisms of drop breakup

The results described in the previous sections are for drop breakup in a high speed airstream. The high speed air is created by a shock wave in a shock tube; the fluid dynamics of compressed, hot gas behind the shock after it has passed over the drop is the disturbing factor responsible for drop fragmentation. The passage of the shock over the drop has no important

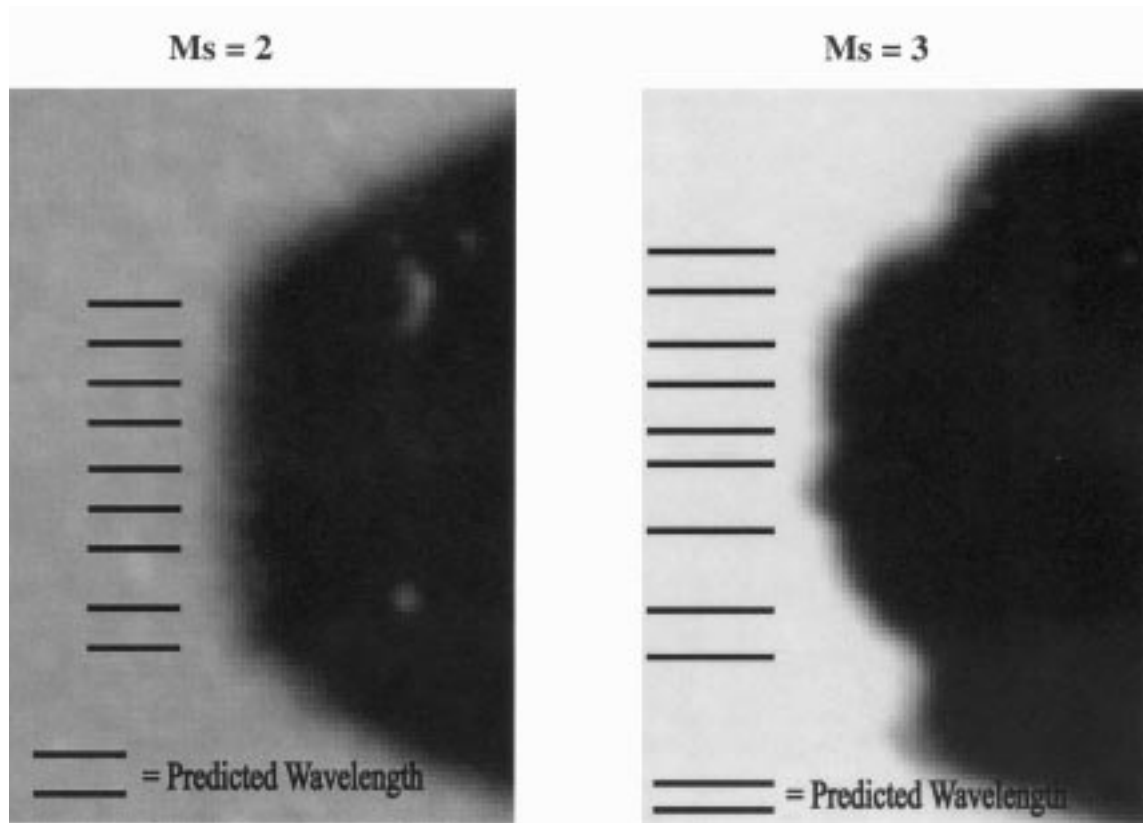


Fig. 20. Rayleigh–Taylor waves in silicone oil (0.1 kg/m s). The tick marks on the photographs locate wave troughs.

influence on breakup. The Mach number of the shock is important indirectly, since it determines the dynamic and thermodynamic state of the gas next to the drop.

It is important to know that drops will not break if the slip velocity is zero. Until a drop breaks up it will accelerate so that its velocity is eventually the same as the air around it; in this case the forces required to break a drop will vanish.

In general, other things being equal, small drops will resist breaking, high surface tension drops will resist breaking, and low dynamic pressure will prevent breaking. This problem was studied by Taylor (1949) who looked at the breakup of 2–5 mm drops subjected to high speed air from a gun blast in tests at Porton Chemical Defense Experimental Establishment. Using heuristic theoretical arguments, he found that the drops of radius D would burst whenever

$$\frac{\rho V^2 D}{4\gamma} > c \text{ (constant)} \approx 2.7 \quad (37)$$

Later research by various people on the breakup of low viscosity Newtonian liquids established that there is a critical Weber number about 12 below which drop breakup does not occur, in agreement with Eq. (37).

It is generally agreed that the minimum critical Weber number increases with the viscosity of

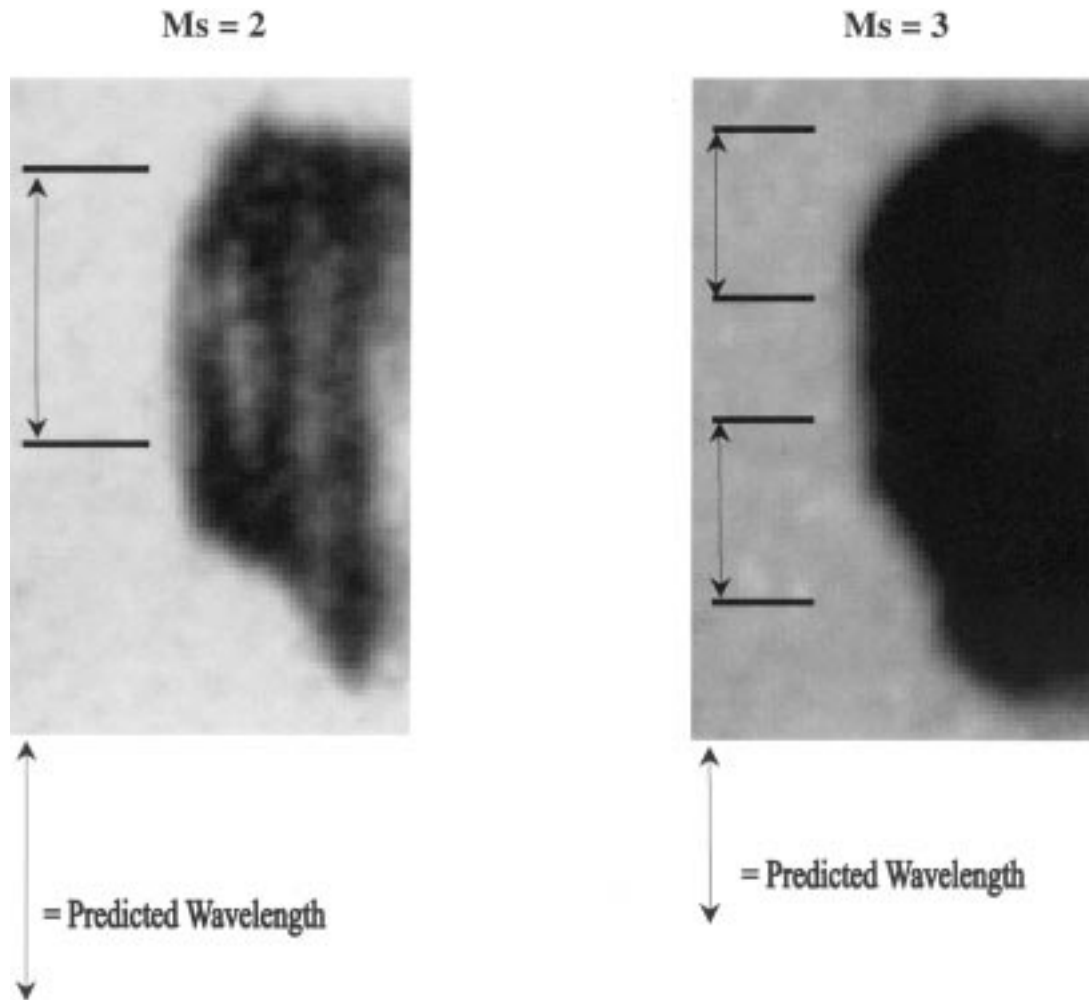


Fig. 21. Rayleigh–Taylor waves in silicone oil (1 kg/m s). The tick marks on the photographs locate wave troughs.

the drop; this dependence is usually expressed through the Ohnesorge number $Oh = \mu_d / (\rho_d D \gamma)^{1/2}$. Brodkey's (Brodkey, 1969) correlation $We = 12(1 + 1.077 Oh^{1.6})$ ($Oh < 5$, $We < 60$) is frequently cited; a similar correlation can be found in Fig. 1 of the paper by Hsiang and Faeth (1992), $Oh < 5$, $We < 200$. The restriction of these correlations to values of $Oh < 5$ is due to the fact that there are apparently very few data on the speed of the relative velocity at final breakup and the drop size; Hsiang and Faeth (1992) say that "...due to the problems of observing drops after secondary breakup there is very little information available about the outcome of secondary breakup..." The $We(Oh)$ curve of the correlation of Brodkey rises so rapidly, when Oh is near to 4, that reliable extrapolation to higher Oh is impossible.

Hsiang and Faeth (1992) attribute the absence of breakup at $Oh > 4$ to a stabilizing effect of viscosity. The issue of stability of a drop of high viscosity may be confused with the effect of high viscosity in delaying the time of breakup. If the delay is great, the drop will accelerate to

Table 4

Comparison of measured breakup times (μs) with predicted times calculated from Eq. (36) with $M = 10$ and using the values of n derived for the fully viscous flow (Table 3)

Liquid	Viscosity (kg/m s)	Shock Mach No. = 3				Shock Mach No. = 2			
		n (s^{-1})	Time for $A = 10A_0$ (μs)	Experimental		n (s^{-1})	Time for $A = 10A_0$ (μs)	Experimental	
				Diameter (mm)	Blow-off (μs)			Diameter (mm)	Blow-off (μs)
Water	0.001	149,632	15	2.6	15	50,971	45	2.5	25
SO 100	0.1	132,198	17	2.6	15	52,727	44	2.6	40
SO 1000	1	48,769	47	2.6	40	20,019	115	2.6	85
Glycerine	1.49	38,760	59	2.4	45	25,046	92	2.4	110
SO 3000	3	31,508	73	2.6	55	14,388	160	2.6	140
SO 4000	4	32,550	71	2.5	65	9868	233	2.5	100 ^b
SO 4000	4			2.1	45 ^a				
Bag breakup					Bag bursting				Bag bursting
SO 4000	4			2.1	195 ^a			2.5	580 ^b
SO 5000	5	24,788	93	2.5	265				
SO 6000	6	24,674	93	2.6	270			2.6	590
SO 10000	10	17,790	129	2.6	370			2.5	860
Viscoelastic					Start of disintegration				Start of disintegration
2% PAA	0.96	61,949		3.2	60				
2.6% PSBA	1.13			2.2	60			2.2	100
2% PO	35	22,807		2.9	60			2.9	110

^a At a Mach number of 3 a 2.5 mm drop of SO 4000 oil begins blow-off at $t = 65 \mu\text{s}$ and continues to break up, whereas a 2.1 mm diameter drop starts to exhibit blow-off at $t = 45 \mu\text{s}$ for a short time and then ceases breakup until it undergoes bag breakup at $t = 195 \mu\text{s}$.

^b A 2.5 mm drop of the same oil exhibits a similar effect at a Mach number of 2.

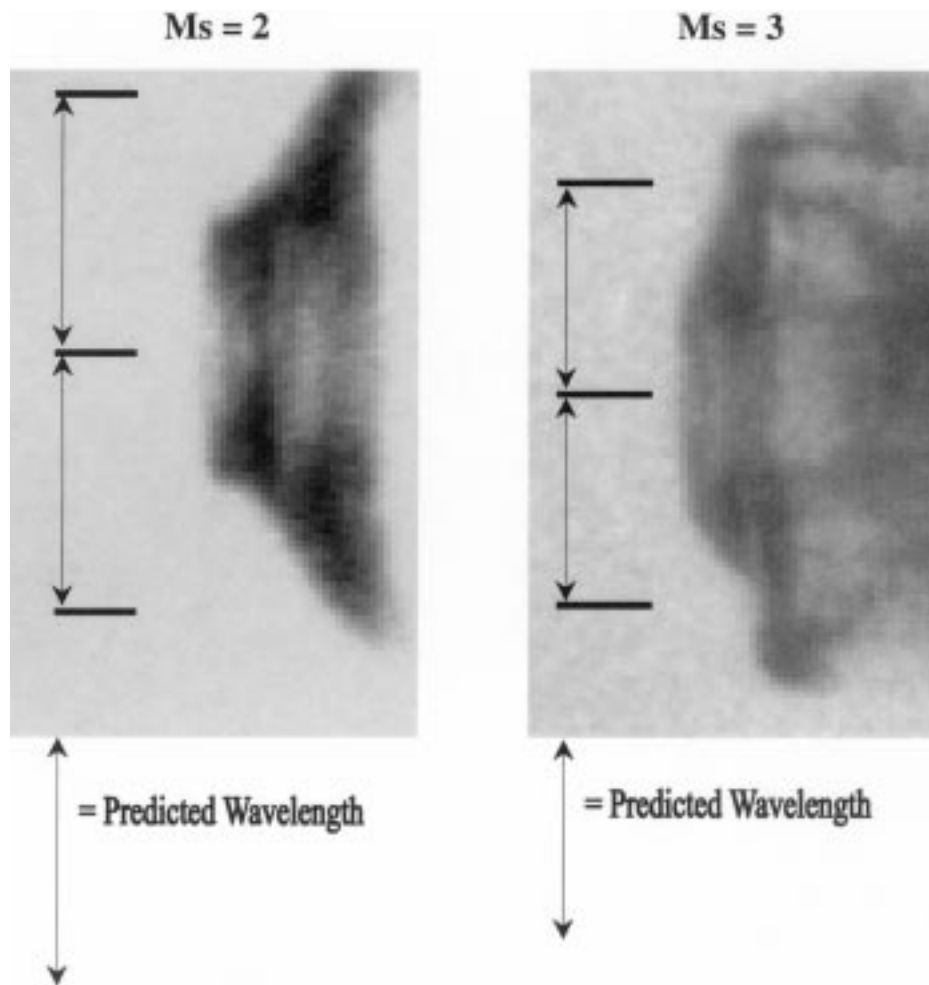


Fig. 22. Rayleigh–Taylor waves in glycerine. The tick marks on the photographs locate wave troughs.

the stream value before it can break. If the relative (slip) velocity between a very viscous drop and the stream around it could be fixed, we might find values, even low values, for We at breakup.

Many mechanisms of instability can lead to fragmentation of drops (see Fig. 15 and the discussion in Hsiang and Faeth (1992)); however, in the present series of high Weber number experiments the main mechanism for breakup appears to be associated with a Rayleigh–Taylor instability driven by ultra high drop accelerations. This instability pumps fingers of hot air, heated by the passing shock wave, into the drop. The fingers inflate the drop like a balloon and at the same time bring hot air into contact with all interior parts of the drop. The drop can break explosively like a balloon, as shown in Fig. 12 for silicone oil.

We have argued that the conditions of very high Weber number ($We > 10,000$) breakup ought to be dominated by Rayleigh–Taylor instability, because the drop accelerations are so large (see Table 2). The agreements of first principle theory and our experiments are

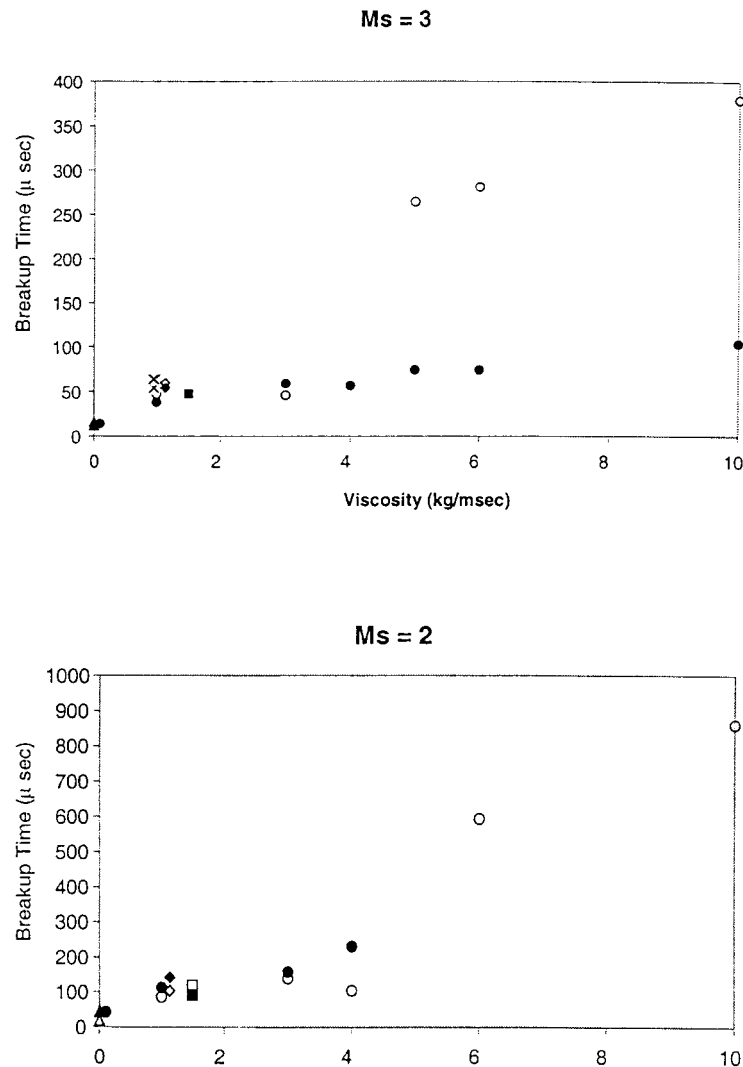


Fig. 23. Time (μs) to blow-off of fluid accumulated at the equator vs. viscosity. The open symbols and crosses are for observed data. The filled symbols are times \hat{t}_b for an unstable disturbance to grow to 10 times its initial value ($\hat{t}_b = 1/n \ln M$, where $M = 10$ and n is the maximum growth rate (s^{-1}) given in Table 3.) For viscosities $\mu \leq 40 \text{ kg/m s}$ the wave length that makes n maximum is less than the drop diameter. These values of n cannot be achieved when $\mu \geq 5 \text{ kg/m s}$; the available growth rates are for waves shorter than the most dangerous one. The shorter waves have much smaller growth rates; this may explain why the observed times of breakup for $\mu > 50 \text{ kg/m s}$ are so much longer than the time to breakup of the unavailable wave of maximum growth.

surprisingly good; we could not point to any feature of the experiments which are in gross conflict with the theory. The quantitative comparisons of predicted with observed wave lengths are excellent, and the use of the growth rate n to predict an initial break-up time (blow-off) $\hat{t}_b = 1/n \ln M$, with $M = 10$ and n given by Eq. (18) for mobile liquids is also an arguably correct semi-theoretical prediction of breakup times for very high Weber number Rayleigh–Taylor breakup.

Finally, it is of interest to compare Rayleigh's Weber number breakup criterion (37) with the criterion (33) when $\lambda = D$ and

$$D < 2\pi \sqrt{\frac{\gamma}{\rho_2 a}} \quad (38)$$

where a is the acceleration giving the drop diameter that is stable against Raleigh–Taylor instability. This criterion leads to values Eqs. (34) and (35) which are not unreasonable. The criterion (38) can be described as a Weber number criterion based on the acceleration

$$\frac{\rho_2 D^2 a}{4\gamma} < \pi$$

identical to criterion (37) when $a = V^2 \pi / 2.7D$. Obviously, the identification of drop sizes after breakup with the wave lengths of unstable waves is not proven and is open to controversy.

8. Summary

- We studied breakup of drops of Newtonian and viscoelastic fluids of about one millimeter diameter in a high speed airstream behind a shock wave in a shock tube.
- Twelve fluids with viscosities ranging from 0.001 to 35 kg/m s were tested at air Weber numbers from 11,700 to 16,900, Ohnesorge numbers from 0 to 82.3 and Reynolds numbers from 40,000 to 127,600.
- High speed movies, posted on our URL, were made with a rotating drum camera giving one photograph every 5 μ s.
- The movies allow one to correlate breakup events with times to the event. The times increase with viscosity.
- Events of short duration which escape attention are captured in the movie. At early times, less than 100 μ s, there is an accumulation of fluid driven by the wind impacting on the windward face to the equator of the drop. The accumulated fluid forms a ring, like Saturn's ring, connected to the drop by a web of liquid, with a lifetime less than 10 μ s.
- Bag-and-stamen in bag breakup occurs routinely at Weber numbers of 0 (10^4 – 10^5) in the higher viscosity drops showing that the presently accepted classification of breakup events, based mainly on water, does not hold generally.
- The early events of breakup (< 100 μ s), flattening, and the accumulation of fluid driven away from the stagnation points, followed by fingering are universal and apply equally to low and high viscosity fluids and to viscoelastic fluids.
- At later times, the drop fragments in viscoelastic fluid are much more stringy than in Newtonian fluids of comparable viscosity. This confirms that the stringiness of drop fragments persists in high speed, high Weber number flows.
- The movies generate time–displacement data from which accelerations of the drop may be computed. The accelerations are 10^4 – 10^5 times the acceleration of gravity, putting the drops at risk to Raleigh–Taylor instabilities.
- Raleigh–Taylor instabilities are computed with an exact viscous theory and with a

simplified theory based on viscous potential flow. It is assumed that the most dangerous wave is the one whose length gives the maximum growth rate. The simplified theory gives the critical wave length and growth rate within a few percent.

- The length of the most dangerous wave increases strongly with viscosity; viscosity should not be neglected as it is in current practice of the atomization community.
- By enhancing the images of drops on photographs from our movies, we are able to identify the wave troughs, to measure the wave on the windward face of the drop at early times.
- We compared theory with experiment using only measured data with no adjustments and found excellent agreement for all cases in which the wave length of the most dangerous mode is less than the drop diameter.
- When the wave length is of the order of the drop diameter, bag breakup is observed. We interpret this bag breakup to arise from a Rayleigh–Taylor instability to long waves (longer than the drop diameter). More viscous drops, with still longer than critical wave lengths undergo a delayed bag breakup.
- When the wave that maximizes the growth rate is longer than the drop diameter, all the unstable waves are longer than critical and the growth rates of these waves is much smaller than critical. Hence, the time to breakup increases with viscosity with very large increases for the cases in which the critical wave is shorter than the drop diameter. This interpretation fits the observed data.
- The border of instability (27) to Rayleigh–Taylor fingers is independent of viscosity; $\lambda_c = 2\pi\sqrt{\gamma/\rho a}$, where a is drop acceleration and γ is the surface tension. Short waves with $\lambda < \lambda_c$ do not lead to fingers. For our experiment, λ lies between 23 and 65 μm for a shock Mach number of 3 and between 46 and 135 μm for a shock Mach number of 2.
- The cutoff value λ_c may be interpreted as a Weber number criterion based on acceleration and $\lambda < \lambda_c \sim D < D_c$ the final values of drop diameters D smaller than those which arise from Rayleigh–Taylor breakup.
- It is suggested that the conventional correlations of drop size with Ohnesorge number are greatly influenced by the fact that the high viscosity drops do not break before they are accelerated to nearly the free stream velocity. When the slip velocity is too small, the drops will not break up and if the slip velocity could be maintained these viscous drops would be reduced to diameters smaller than those in the correlations.
- The observed events at high Weber numbers seem to be consistent with every aspect of Rayleigh–Taylor stability analysis. This suggests that the dynamics of breakup at high Weber numbers is controlled by the huge drop accelerations at early times when the drop is nearly stationary.

Acknowledgements

The authors acknowledge the valuable contributions of Gerry Brenden, Kristen Alberts, Abby Eichman, and Paul Hannah.

This work was supported by US Army ERDEC through Grant No. Battelle/135905-1/Army, by the Army Research Office and by the National Science Foundation under grant 9622235.

References

- Brodkey, R.S., 1969. *The Phenomena of Fluid Motions*. Addison Wesley, Reading, MA.
- Chandrasekhar, S., 1961. *Hydrodynamic and Hydromagnetic Stability*. Clarendon Press, Oxford.
- Davies, R.M., Taylor, G.I., 1950. The mechanics of large bubbles rising through extended liquids and through liquids in tubes. *Proc. Roy. Soc. (London)* A200, 375–390.
- Engel, O.G., 1958. Fragmentation of waterdrops in the zone behind an air shock. *J. Res. Natl. Bur. Stand.* 60, 245–280.
- Faeth, G.M., 1996. Spray combustion phenomena. In: *Twenty-Sixth Symposium on Combustion*, The Combustion Institute, 1593–1611.
- Hanson, A.R., Domich, E.G., 1956. The effect of viscosity on the breakup of droplets by air blasts — a shock tube study. Research Report No. 130, Department of Aerospace Engineering, University of Minnesota, Minneapolis, MN.
- Hanson, A.R., Domich, E.G., Adams, H.S., 1963. Shock tube investigation of the breakup of drops by air blasts. *Phys. Fluids* 6, 1070–1080.
- Harrison, W.J., 1908. The influence of viscosity on the stability of superposed fluids. *Proc. London Math Soc.* 6, 396–405.
- Hirahara, H., Kawahashi, M., 1992. Experimental investigation of viscous effects upon a breakup of droplets in high-speed air flow. *Exp. in Fluids* 13, 423–428.
- Hsiang, L.P., Faeth, G.M., 1992. Near-limit drop deformation and secondary breakup. *Int. J. Multiphase Flow* 18, 635–652.
- Hwang, S.S., Liu, Z., Reitz, R.D., 1996. Breakup mechanisms and drag coefficients of high-speed vaporizing liquid drops. *Atomization and Sprays* 6, 353–376.
- Joseph, D.D., 1994. Potential flows of viscous and viscoelastic fluids. *J. Fluid Mech.* 265, 1–23.
- Joseph, D.D., Saut, J.C., 1990. Short-wave instabilities and ill-posed initial-value problems. *Theoretical Comput. Fluid Dynamics* 1, 191–227.
- Joseph, D.D., Huang, A., Candler, G.V., 1996. Vaporization of a liquid drop suddenly exposed to a high-speed airstream. *J. Fluid Mech.* 318, 223–239.
- Kitscha, J., Kocamustafaogullari, G., 1989. Breakup criteria for fluid particles. *Int. J. Multiphase Flow* 15, 573–588.
- Krzczkowski, S.A., 1980. Measurement of liquid droplet disintegration mechanisms. *Int. J. Multiphase Flow* 6, 227–239.
- Lane, W.R., 1951. Shatter of drops in stream of air. *Ind. Eng. Chem.* 43, 1312–1317.
- Levich, V.G., 1949. The motion of bubbles at high Reynolds numbers. *Zh. Eksp. Teor. Fiz.* 19, 18.
- Lewis, D.J., 1950. The instability of liquid surfaces when accelerated in a direction perpendicular to their planes: Part II. *Proc. Roy. Soc.* A117, 81–96.
- Matta, J.E., Tytus, R.P., 1982. Viscoelastic breakup in a high velocity airstream. *J. Appl. Polymer Science* 27, 397–405.
- Matta, J.E., Tytus, R.P., Harris, J., 1983. Aerodynamic atomization of polymeric solutions. *Chem. Eng. Commun.* 19, 191–204.
- Pilch, M., Erdman, C., 1987. Use of break-up time data and velocity history data to predict the maximum size of stable fragments for acceleration-induced break-up of a liquid drop. *Int. J. Multiphase Flow* 13, 741–757.
- Plesset, M.S., Prosperetti, A., 1977. Bubble dynamics and cavitation. *Ann. Rev. Fluid Mech.* 9, 145–185.
- Ranger, A.A., Nicholls, J.A., 1969. Aerodynamic shattering of liquid drops. *AIAA J.* 7, 285–290.
- Reinecke, W.G., McKay, W.L., 1969. Experiments on water drop breakup behind Mach 3 to 12 shocks. AVTD-0172-69-RR, AVCO Corp.
- Reinecke, W.G., Waldman, G.D., 1970. A study of drop breakup behind strong shocks with applications to flight. SAMS0-TR-70-142, Avco Systems Division.
- Reinecke, W.G., Waldman, G.D., 1975. Shock layer shattering of cloud drops in reentry flight. *AIAA Paper* 75-152.
- Simpkins, P.G., Bales, E.L., 1972. Water-drop response to sudden accelerations. *J. Fluid Mech.* 55, 629–639.
- Stone, H.A., 1994. Dynamics of drop deformation and breakup in viscous fluids. *Annual Rev. Fluid Mech.* 26, 65–102.
- Taylor, G.I., 1949. The shape and acceleration of a drop in a high-speed air stream. *Advisory Council on Scientific*

- Research and Technical Development, Ministry of Supply, AC 10647/Phys. C69; also in *The Scientific Papers of G.I. Taylor 3*, (Batchelor, G.K. (Ed.)), University Press, Cambridge, 1993.
- Taylor, G.I., 1950. The instability of liquid surfaces when accelerated in a direction perpendicular to their planes, Part I. *Proc. Roy. Soc. A*, 201, 192–196; also in *The Scientific Papers of G.I. Taylor 3*, (Batchelor, G.K. (Ed.)), University Press, Cambridge (1993).
- Waldman, G.D., Reinecke, W.G., Glenn, D., 1972. Raindrop breakup in the shock layer of a high-speed vehicle. *AIAA J.* 10, 1200–1204.
- Wierzbna, A., 1990. Deformation and breakup of liquid drops in a gas stream at nearly critical Weber numbers. *Experiments in Fluids* 9, 59–64.
- Wierzbna, A., Takayama, K., 1988. Experimental investigation of the aerodynamic breakup of liquid drops. *AIAA J.* 26, 1329–1335.
- Wilcox, J.D., June, R.K., Braun, H.A., Kelly, R.C., 1961. The retardation of drop breakup in high-velocity air-streams by polymeric modifiers. *J. App. Polymer Sci.* 5 (13), 1–6.
- Yoshida, T., Takayama, K., 1990. Interaction of liquid droplets with planar shock waves. *Trans. ASME, J. Fluids Eng.* 112, 481–486.